NASA TECHNICAL MEMORANDUM

NASA TM X-1135

PRESSURE DISTRIBUTION ON HL-10 MANNED LIFTING ENTRY VEHICLE AT A MACH NUMBER OF 19.5

by William D. Harvey
Langley Research Center
Langley Station, Hampton, Va.

NATIONAL AERONAUTICS AND SPACE ADMINISTRATION • WASHINGTON, D. C. • SEPTEMBER 1965

NASA TM X-1135

PRESSURE DISTRIBUTION ON HL-10 MANNED LIFTING ENTRY VEHICLE AT A MACH NUMBER OF 19.5

By William D. Harvey

Langley Research Center
Langley Station, Hampton, Va.

NATIONAL AERONAUTICS AND SPACE ADMINISTRATION

PRESSURE DISTRIBUTION ON HL-10 MANNED LIFTING ENTRY VEHICLE AT A MACH NUMBER OF 19.5*

By William D. Harvey
Langley Research Center

SUMMARY

An experimental investigation has been conducted to determine the pressure distribution on the lower surface of the basic reentry configuration (designated HL-10 by the Langley Research Center) having a hypersonic maximum lift-drag ratio of about 1.0. Tests were made in the Langley hotshot tunnel at a Mach number of 19.5 and free-stream Reynolds number per foot of about 0.48×10^6, for angles of attack from 15° to 50°, and elevon deflections of 0°, 15°, and 30°.

A comparison of measured pressures and values derived from Newtonian theory agree along the curved lower surface for angles of attack up to 30°. For larger angles of attack, the experimental pressures were higher than the theoretical pressures for the forward portions of the model. The data obtained from limited tests with a smaller model showed improvement in the comparison of experiment and theory.

A 30° downward deflection of the trailing-edge elevons caused apparent laminar separation to occur at angles of attack of 40° and 50° (and perhaps 30°). Improved predictions of elevon pressures were obtained by use of embedded flow theory rather than Newtonian theory. The tip-fin leading-edge pressure level decreased with increasing angle of attack.

INTRODUCTION

Recent studies of manned lifting entry vehicles (see, for example, ref. 1) have directed increased attention to the potential use of vehicles with a hypersonic lift-drag ratio of about 1. At the Langley Research Center studies were undertaken to define the problems and probable solutions associated with this type of entry vehicle and to develop a configuration for detailed studies. From these studies, the HL-10 configuration has evolved; reference 2 contains a summary of the concepts behind the vehicle design.

---

*Title, Unclassified.

References 2 to 4 present results from some of the experimental investigations made to determine aerodynamic force and stability characteristics. From these studies, a basic configuration with canted tip fins and central dorsal fin (tip fin D and central dorsal fin E described in refs. 3 and 4) has evolved. Reference 5 presents some aerodynamic characteristics at Mach 20. Reference 6 presents laminar heat-transfer characteristics of the basic configuration, whereas reference 7 presents the turbulent heating results for this model.

The purposes of the present investigation were (1) to determine the pressure distribution over the lower surface of the basic vehicle which may possibly aid in the prediction of the heat-transfer rate, (2) to determine the adequacy of Newtonian impact theory in predicting the pressures, and (3) to provide information for structural studies. Two pressure models of the HL-10 (using tip fins D of reference 4 but without a central dorsal fin) were tested in the Langley hotshot tunnel at a nominal Mach number of 19.5 and a free-stream Reynolds number per foot of 0.48×10^6. One model had a maximum chord length of 8 inches and the other, 6 inches. Chordwise and spanwise pressure distributions over the lower surface of the 8-inch model were determined at angles of attack of 15°, 20°, 30°, 40°, and 50° with elevon deflections of 0°, 15°, and 30°. For comparison with the 8-inch-model pressure data the chordwise pressure distributions over the lower surface of the 6-inch model were determined at angles of attack of 30°, 40°, and 50° with 0° elevon deflection. The data for both models were compared with the Newtonian pressure theory.

SYMBOLS

C_p pressure coefficient, $\frac{p_w - p_\infty}{q_\infty}$

c maximum chord, inches

D_n nose diameter, inches

M_∞ free-stream Mach number

p_t total pressure, lb/sq in.

p_w wall pressure, lb/sq in.

p_∞ free-stream static pressure, lb/sq in.

q_∞ free-stream dynamic pressure, lb/sq in., $\frac{1}{2}\rho_\infty V_\infty^2$

R_∞ free-stream Reynolds number per foot, $\frac{\rho_\infty V_\infty x}{\mu_\infty}$

T_t total temperature, ^oR

T_∞ free-stream temperature, ^oR

s surface distance from plane of symmetry, inches

V_∞ free-stream velocity, feet per second

x,y,z model coordinates (See fig. 1 and table I.)

α angle of attack, degrees

β angle between tangent to body surface and free-stream flow, degrees

γ ratio of specific heats

δ_e elevon deflection angle in plane normal to hinge line, positive when trailing edge is down, degrees

μ_∞ free-stream viscosity, lb/ft-sec

ρ_∞ free-stream density, lb/cu ft

APPARATUS AND TESTS

Tunnel

The present investigation was conducted in the Langley hotshot tunnel. This tunnel is similar to other hotshot tunnels in that a high-energy arc is discharged within a chamber to heat and pressurize the test gas. Upon rupture of a diaphragm upstream of the nozzle throat, the nitrogen expands through a conical nozzle and the test section into a vacuum reservoir. A more detailed description of the tunnel can be found in reference 8. The arc chamber used in the present tests is the coaxial electrode arrangement described in appendix A of reference 8 without the magnetic coil. Nominal test conditions for the present investigation are as follows:

γ	7/5
M_∞	19.5
R_∞	0.48×10^6
p_t, psia	10,000
p_∞, psia	0.0018
T_∞, ^oR	61.5
T_t, ^oR	4230

Instrumentation

Pressure measurements on the model surfaces were made with single-diaphragm variable-reluctance transducers. They were rated at 0.25, 0.5, and 1 pound per square inch full scale and located with respect to the anticipated pressure level along the model surface. Figures 2 and 3 show the pressure-orifice locations and their spanwise and chordwise locations are given in table II. Nine gages (gages 1 to 9) were located along the center line of the lower surface with seven gages (gages 10 to 16) on the outboard ray, just inboard of the point of tangency between the leading edge and the bottom surface. A ray of four gages (gages 22 to 25) was located just ahead of one elevon and three gages (gages 26 to 28) were located on the elevon. Another ray of gages (gages 17 to 22) was located along the side of the model. (See fig. 2(a).) Three orifices (gages 29 to 31) were located on the leading edge of one tip fin. (Shown in figure 3 but not in figure 2.) All transducers were referenced to a common manifold installed in the model. The 6-inch model was instrumented only along the center line at approximately the same chordwise stations as the 8-inch model.

The short tunnel-operation-time and the low pressures to be measured required that the pressure transducers be mounted within the model to avoid excessive lag in the measurements. The number of transducers and orifices was therefore limited by the internal volume of the model. Calibration of each pressure transducer was performed over the pressure range anticipated for each test. The linear calibration could be repeated with an accuracy of ±5 percent.

The total pressure in the arc chamber (see ref. 8) was measured with strain-gage pressure transducers during each test. Total pressure behind the normal shock in the test section was measured with variable-reluctance pressure transducers.

Pressure data were obtained by recording the amount of deflection with time on an oscillograph. Prior to the tests, a calibration of the pressure range anticipated was made for the individual gages. Measurements were read from the oscillograph records at 10-millisecond intervals with the first indication of a pressure rise selected as zero time.

Models

A drawing of the 8-inch model of the basic HL-10 configuration used for the present investigation is shown in figure 1. The configuration tested had the canted tip fins (fin D of ref. 4) that provide directional stability primarily at high angles of attack at supersonic and hypersonic speeds. The vertical fin (ref. 3) was not used to permit sting mounting the model. A table of body coordinates (tip fins and vertical tail not included) for the model is given in table I. The coordinates for the smaller configuration (6-inch model) were obtained by multiplying the 8-inch model coordinates given in table I by 3/4.

Essentially, the lower surface of the model is a blunt-leading-edge delta wing with negative camber. The nose diameter (0.75 inch) of the HL-10

configuration is equal to the cylindrical leading-edge diameter, although the leading edge is of constant radius for only about 90° of arc beginning on the lower surface. This leading-edge diameter is faired into the curved upper surface. The lower surface is flat in the spanwise direction and has curvature only in the chordwise direction. The sweep angle is 74°.

The fiber glass models consist of an upper and lower surface with cutouts for elevon installation. Pressure orifices were located, the two halves were assembled, and the elevons were attached separately. Photographs of the finished 8-inch model are shown in figure 2.

The elevons were constructed of stainless steel bent to the desired deflection angles and then bonded to a block of wood. This type of construction resulted in the deflected solid elevon shown schematically in figure 1. A removable hatch, shown in figure 2(a), was provided for installation of pressure instrumentation.

The model support sting entered the top of the model near the rear. (See figs. 1 and 2.) The sting was attached to a mounting block which in turn was fastened to the interior floor with screws along the center line of the model.

Tests and Data Reduction

Calibration data for the tunnel test section and nozzle are given in reference 8. The nominal stagnation pressure and temperature for the present investigation were approximately 10 000 psia and 4230° R. The corresponding free-stream Mach number and Reynolds number per foot were 19.5 and 0.48×10^6, respectively.

It has been the practice to define the flow by measuring simultaneously the test-section pitot pressure and the reservoir pressure and, the density of the initial charge of gas in the reservoir being known, to assume that the same density, uniformly distributed, existed in the reservoir after arc discharge. With these three parameters, it was possible to calculate all the other characteristics of the flow by using a suitable data reduction program such as that in reference 9.

Prior to the present investigation a series of tunnel tests were made in which simultaneous measurements of free-stream velocity, stagnation-point heat-transfer rate, and the previously mentioned pressures and density were obtained to evaluate the assumption of uniform density. These results yield correction factors which may be applied to test results for which the density was assumed to be uniformly distributed. Therefore, the stagnation temperature, free-stream temperature, and Reynolds number for the present investigation were modified by a series of time-dependent correction factors to account for the nonuniform density distribution.

The ratio of the measured pressure to the free-stream pressure p_w/p_∞ was substituted into the expression for the local pressure coefficients C_p, defined as

$$C_p = \frac{2}{\gamma M_\infty^2}\left(\frac{p_w}{p_\infty} - 1\right) \tag{1}$$

THEORY

In order to assess the predictability of the pressure level and distribution, theoretical values were calculated for various portions of the configuration and were compared with the experimental data for angles of attack of 15°, 20°, 30°, 40°, and 50° for elevon deflections of 0°, 15°, and 30°. Newtonian approximations of the pressure coefficients on the model of the present investigation were obtained with the use of the expression

$$C_p = 2 \sin^2\beta \tag{2}$$

In order to obtain chordwise pressure distributions along the center line and outboard rays, the local surface angles along the lower surface of the model were measured and added to the various angles of attack. These angles were then substituted into equation (2) to determine the local pressure coefficients for the various angles of attack.

Pressures on the elevons were estimated by two methods. Newtonian calculations were made by substituting the angle between the deflected elevon surface and the flow direction into equation (2) for each angle of attack. Calculations were also made for the deflected elevons by using the method of reference 10. Reference 10 presents results indicating that for hypersonic flow fields having secondary shock waves generated by ramps that are embedded within the main disturbed flow field, the pressure coefficients in the embedded region can be considerably different from those obtained by simple Newtonian impact theory. Equation (2) of reference 10 may be written as

$$C_{p,2} = C_{p,1} + 2\,\frac{p_1 M_1^2}{p_\infty M_\infty^2} \sin^2\delta_e \tag{3}$$

where $C_{p,2}$ represents the pressure coefficient on the deflected elevon, $C_{p,1}$ and p_1 represent the Newtonian pressure coefficient and pressure on the model center line at the same chordwise station as the elevon hinge line, and M_1 represents the Mach number at the hinge line calculated from the Newtonian pressure p_1 and the maximum Newtonian pressure coefficient (which has a value of 2).

To obtain the spanwise pressure distribution, cross sections were taken at various chordwise stations along the body. These stations were located at x/c values of 0.125, 0.262, 0.373, 0.484, 0.625, 0.763, and 0.886. Spanwise pressure distributions were calculated by use of equation (2) and a computer program using the model cross-sectional coordinates from table I. The normal to each coordinate and the Newtonian angles were found by the method of direction

cosines, and the local pressure coefficients were computed for the various spanwise stations.

RESULTS AND DISCUSSION

Schlieren photographs are presented as figure 4. (Dark spots on the photographs are chips in the test-section windows.) The free-stream flow direction is from left to right. The schlieren flow-field details, although not extremely clear, can be used in conjunction with the pressure measurements to evaluate the existence of separated flow. It is believed that laminar separation existed at the present test conditions for the 30° elevon deflection at angles of attack of 40° and 50° with a possibility of separation at 30°. Figures 5 to 10 give the pressure distributions for elevon deflections of 0°, 15°, and 30°.

Chordwise Pressure Distributions

Chordwise pressure distributions along the center line of the lower surface, along the ray ahead of the elevon, and along the elevon are presented in figures 5(a), 7(a), and 9(a) for various angles of attack. The solid symbols represent data from the 6-inch model. The flagged symbols represent the data for the ray ahead of the elevon and on the elevon; unflagged symbols represent the center-line ray. Newtonian pressure coefficients are shown in each figure for all angles of attack. Figures 5(b), 7(b), and 9(b) are corresponding plots of the outboard ray pressure distribution.

Without elevon deflection.- In general, the theory agrees well with the experimental results for the 8-inch model for angles of attack of 15° and 20° (fig. 5(a)). At $\alpha = 30°$, the data are about 40 percent higher than theory at the 6-percent chord and at $\alpha = 40°$, about 25 percent higher than theory for the same chordwise station. However, the agreement between experimental pressure coefficients and theory is good for the remaining chordwise stations. At $\alpha = 50°$, the experimental pressures are about 10 percent higher than theory from about the 10-percent chord to the 40-percent chord. The exact cause of this difference between the experimental data and theory is not known. An earlier investigation (ref. 5) in the same facility to obtain force and moment characteristics on the HL-10 configuration yielded somewhat similar results in that the pitching-moment coefficients at the maximum angles of attack were higher than those obtained in other hypersonic investigations. (See fig. 7 of ref. 5 for a comparison of stability characteristics.) Consideration was given to whether the 8-inch model could have induced partial blockage of the flow at $\alpha = 50°$ although the schlieren photographs (fig. 4) did not support such a possibility. To investigate the possibility of blockage, additional tests were made with a 6-inch model (having a frontal area nine-sixteenths of that of the 8-inch model) at angles of attack of 30°, 40°, and 50°, and with $\delta_e = 0°$. The 6-inch model had a single row of pressure orifices along the center line of the lower surface at the same chordwise stations as the 8-inch model. The tests with the 6-inch model gave results similar to those obtained with the 8-inch model in that the experimentally determined pressures on the 6-inch model were also approximately 10 percent higher than the theoretical values for $\alpha = 50°$ from about the 10-percent chord to the 20-percent chord. (See fig. 5(a) for a

comparison of the 6- and 8-inch-model pressure data.) However, the experimental data for the 6-inch model at $\alpha = 50^\circ$ between the 25-percent chord and the 40-percent chord indicate better agreement with theory than the 8-inch model. For angles of attack of 30° and 40°, the 6-inch model shows good agreement with theory from the 6-percent chord to the 100-percent chord. Therefore, it appears that if a blockage effect exists at high angles of attack with the large model, it is somewhat reduced with the smaller model for chordwise stations between the 25-percent chord and the 40-percent chord. Because the stagnation point moved aft as the angle of attack increased, the pressure orifice located at the nose (see table II and fig. 3) indicates a decrease in pressure with increasing angle of attack as expected. Likewise, the pressure increases for gages located at x/c values of 0.060, 0.125, and 0.262 with increasing angle of attack. No separation is indicated by the experimental pressures for $\delta_e = 0^\circ$.

In figure 5(b), the outboard-ray pressure distribution also agrees with theory for all angles of attack except 50° where a disagreement exists up to about the 50-percent chord as was seen in figure 5(a).

With elevon deflection.- With the elevon deflected 15° (fig. 7(a)), the measured pressure distributions over the first 40 percent of the body were similar to those of figure 5(a) with $\delta_e = 0^\circ$, and the same discrepancies between measurements and theory are noted. The pressure level ahead of the elevons indicates that the flow is separated on the forward part of the elevon. (The schlieren photographs of fig. 4(a) tend to confirm this separation.) Once again, the outboard ray (fig. 7(b)) shows results similar to figure 5(b) for the experimental data and theory for the various angles of attack.

Figure 9(a) shows the agreement between experimental data and theory and is similar to figures 5(a) and 7(a) up to approximately the 40-percent chord. It is shown in figure 9(a) that the pressure level ahead of the elevon deflected 30° is greater than theory with a further rise on the elevon for angles of attack of 40°, 50°, and possibly for 30°, but not for the lower angles. The pressure rise ahead of the elevon begins at approximately the 70-percent chord. It is believed that the flow is separated ahead of the elevon at angles of attack of 40° and 50° with a possibility of separation for an angle of attack of 30°. A heat-transfer investigation at Mach 8 (ref. 6) indicates that 30° downward deflection of the elevons caused laminar separation on the lower surface. Further indication of this separation at $\alpha = 50^\circ$, may be seen in figure 4, where comparison between the schlieren photographs at $\delta_e = 15^\circ$ (fig. 4(a)) and $\delta_e = 30^\circ$ (fig. 4(d)) indicates the difference between the separated and nonseparated flow on the lower surface. The extent of this separation on the lower surface can be seen by comparing the pressure distribution at $x/c = 0.70$ for the 30° elevon deflection (fig. 9(a)) with the undeflected elevon (fig. 5(a)). A comparison between the experimental results and the pressure coefficients predicted by simple Newtonian theory and the method of reference 10 (embedded-flow theory) may be seen in figures 7(a) and 9(a). The simple Newtonian theory overpredicted the maximum experimental pressure results on the deflected elevons; the method of reference 10 underpredicted the experimental results but still gave considerably better agreement than the simple Newtonian approximation.

The pressure level ahead of the elevon is about the same as that for the center line at the same x/c value (fig. 9(a)). This agreement indicates that the flow is probably separated inboard of the elevons at $x/c \approx 0.70$. Further indication of the spanwise separation at $x/c = 0.70$ can be seen in figure 9(b) where the pressure level has risen with increasing angle of attack for the last two stations ($x/c = 0.763$ and $x/c = 0.886$). Because of the limited number of orifices on the elevon, insufficient data were obtained to determine whether reattachment of the separated flow occurred on the elevons, although from the schlieren photograph (fig. 4(d)) it appears that the flow does reattach on the elevons. Reference 6 points out that a region of higher heating was observed to cross the elevons diagonally near the midchord of the elevons and was believed to result from flow reattachment.

Spanwise Pressure Distributions

The experimental data are plotted for the spanwise pressure distributions along with Newtonian coefficients in figures 6, 8, and 10.

Experimental pressure data for the deflected elevons are not plotted on the figures presenting the spanwise-pressure-distribution. Also, the data for gages 24 ($x/c = 0.736$) and 26 ($x/c = 0.902$) are not included in these figures.

The local pressure coefficient is plotted against the ratio of the surface distance to the nose diameter s/D_n. Theoretical distributions plotted in these figures begin on the center line of the lower surface and extend around the 90°-arc leading-edge station and well up onto the relatively flat top surface of the configuration. (See the respective cross sections in fig. 3.)

It is evident in the experimental pressure data at the x/c values of 0.123 and 0.262 in parts (d) and (e) of figures 6, 8, and 10 for the higher angles of attack that the pressure level on the center line and outboard ray is higher than the theoretical peak pressures on the leading edge for the same chordwise stations. However, the experimental data are in good agreement for the remaining x/c values. This disagreement between the experimental pressure data and theory was mentioned earlier for these stations on the center-line and outboard-ray plots. (See figs. 5, 7, and 9.)

Good agreement is obtained between the experimental spanwise pressure distribution for $\delta_e = 0°$ and theory for x/c values of 0.373, 0.484, 0.625, 0.763, and 0.886. Spanwise pressures for $\delta_e = 15°$ and $\delta_e = 30°$ are shown in figures 8 and 10. These figures also indicate good agreement between experimental pressures and theory as did figure 6, except for the last two chordwise stations ($x/c = 0.763$ and $x/c = 0.886$) which are believed to be in the region of laminar separation.

Tip-Fin Pressure Distributions

Figure 11 is a plot of the tip-fin leading-edge pressure distribution for the various angles of attack. The experimental data are plotted only for

$\delta_e = 0^\circ$ since for the tip-fin leading-edge pressure distribution there was no apparent effect from deflecting the elevons downward 15° or 30°. In general, the pressure level along the tip-fin leading-edge length decreased with increasing angle of attack, as would be expected from isolated-cylinder concepts.

CONCLUSIONS

An investigation to determine the pressure distribution over the underside of the basic version of a manned lifting entry vehicle (designated HL-10) has been performed in the Langley hotshot tunnel for a Mach number of 19.5 and a free-stream Reynolds number per foot of 0.48×10^6. Analysis of the experimental data, and a comparison with theory have resulted in the following conclusions:

(1) With the exception of one chordwise station (6-percent chord) near the model nose at angles of attack of 30° and 40° and four stations (between the 6-percent chord and the 40-percent chord) at angles of attack of 50° for which the experimental results were considerably higher than theory, good agreement was obtained between experimental results and Newtonian approximations for the center line and outboard rays of the lower surface, excluding elevon deflections.

(2) Better agreement between experiment and theory was obtained with a smaller model at the higher angles of attack; thus a partial tunnel blockage may be present with the larger model at high angles of attack.

(3) The experimental pressure distributions on the elevons deflected at 15° and 30° were overpredicted by simple Newtonian theory whereas they were underpredicted by the embedded-flow theory. However, the embedded-flow theory gave better agreement with the experimental pressures.

(4) Downward elevon deflection of 30° caused laminar separation on the lower surface and an apparent reattachment on the elevons for angles of attack of 40° and 50°. Separation appears to occur at approximately the 70-percent chord and extend across the lower surface in the spanwise direction.

Langley Research Center,
National Aeronautics and Space Administration,
Langley Station, Hampton, Va., June 11, 1965.

REFERENCES

1. Love, E. S.; and Pritchard, E. B.: A Look at Manned Entry at Circular to Hyperbolic Velocities. 2nd Manned Space Flight Meeting (Dallas, Texas), Am. Inst. Aeron. Astronaut., Apr. 1963, pp. 167-180.

2. Rainey, Robert W.; and Ladson, Charles L.: Preliminary Aerodynamic Characteristics of a Manned Lifting Entry Vehicle at a Mach Number of 6.8. NASA TM X-844, 1963.

3. Ware, George: Aerodynamic Characteristics of Models of Two Thick 74° Delta Manned Lifting Entry Vehicles at Low-Subsonic Speeds. NASA TM X-914, 1964.

4. Ladson, Charles L.: Aerodynamic Characteristics of a Manned Lifting Entry Vehicle at a Mach Number of 6.8. NASA TM X-915, 1964.

5. Harris, Julius E.: Aerodynamic Characteristics of a Manned Lifting Entry Vehicle at a Mach Number of 19.7. NASA TM X-1080, 1964.

6. Dunavant, James C.; and Everhart, Philip E.: Investigation of the Heat Transfer to the HL-10 Manned Lifting Entry Vehicle at a Mach Number of 8. NASA TM X-998, 1964.

7. Everhart, Philip E.; and Hamilton, H. Harris: Investigation of Roughness - Induced Turbulent Heating to the HL-10 Manned Lifting Entry Vehicle at a Mach number of 8. NASA TM X-1101, 1965.

8. Smith, Fred M.; Harrison, Edwin F.; and Lawing, Pierce L.: Description and Initial Calibration of the Langley Hotshot Tunnel With Some Real-Gas Charts for Nitrogen. NASA TN D-2023, 1963.

9. Grabau, Martin; Humphrey, Richard L.; and Little, Wanda J.: Determination of Test-Section, After-Shock, and Stagnation Conditions in Hotshot Tunnels Using Real Nitrogen at Temperatures From 3000 to 4000°K. AEDC-TN-61-82, U.S. Air Force, July, 1961.

10. Seiff, Alvin: Secondary Flow Field Embedded in Hypersonic Shock Layers. NASA TN D-1304, 1962.

TABLE I.- HL-10 MODEL COORDINATES

[All dimensions are in inches. Coordinates do not include tip or dorsal fins.]

z	y
x = 1	
0.5896	0
.5833	.0664
.5617	.1336
.5281	.2000
.4833	.2640
.4041	.3336
.3336	.3816
.2664	.4224
.2000	.4568
.1336	.4832
.0664	.5056
0	.5248
-.0664	.5400
-.1336	.5528
-.2000	.5632
-.2664	.5712
-.7233	0
x = 2	
0.6458	0
.6426	.0664
.6336	.1336
.6184	.2000
.5984	.2664
.5696	.3336
.5328	.4001
.4848	.4664
.4216	.5336
.3664	.5768
.3336	.6032
.2664	.6490
.2000	.6899
.1336	.7219
.0664	.6855
0	.7719
-.0664	.7923
-.1336	.8090
-.2000	.8218
-.2664	.8352
-.3336	.8455
-.4000	.8538
-.4664	.8608
-.5336	.8666
-.9639	0
x = 3	
0.6567	0
.6560	.0664
.6528	.1336
.6471	.2000
.6392	.2664
.6264	.3336
.6128	.4001
.5952	.4664
.5712	.5336
.5432	.6000
.5064	.6663
.4608	.7335

z	y
x = 3 continued	
.4024	.8000
.3320	.8666
.2664	.9088
.2000	.9498
.1336	.9831
.0664	1.0099
0	1.0336
-.0664	1.0552
-.1336	1.0695
-.2000	1.0867
-.2664	1.1015
-.3336	1.1155
-.4001	1.1264
-.4664	1.1360
-.5336	1.1431
-.6013	1.1495
-.6663	1.1539
-1.0675	0
x = 4	
0.6256	0
.6256	.1336
.6240	.2000
.6208	.2664
.6160	.3336
.6096	.4000
.6008	.4664
.5904	.5336
.5784	.6000
.5640	.6663
.5456	.7335
.5240	.8000
.4960	.8666
.4632	.9338
.4232	1.0003
.3734	1.0663
.3120	1.1335
.2664	1.1667
.2000	1.2167
.1336	1.2570
.0664	1.2896
0	1.3149
-.0664	1.3376
-.1336	1.3555
-.2664	1.3722
-.2000	1.3863
-.3336	1.4003
-.4000	1.4106
-.4664	1.4202
-.5336	1.4279
-.6000	1.4336
-1.0279	0
x = 5	
0.5728	0
.5728	.8320
.5728	.2168
.5704	.3496

z	y
x = 5 continued	
.5656	.4832
.5568	.6168
.5424	.7495
.5240	.8832
.5096	.9498
.4928	1.0163
.4728	1.0835
.4464	1.1495
.4168	1.2160
.3824	1.2832
.3432	1.3498
.2920	1.4163
.2336	1.4739
.2000	1.5027
.1336	1.5527
.0664	1.5930
0	1.6224
-.0664	1.6455
-.1336	1.6640
-.2000	1.6808
-.2664	1.6944
-.3336	1.7056
-.4000	1.7144
-.8584	0
x = 6	
0.4936	0
.4928	.5000
.4920	.6328
.4888	.7667
.4848	.8999
.4768	1.0330
.4648	1.1667
.4488	1.2992
.4264	1.4330
.3904	1.5667
.3664	1.6327
.3368	1.6992
.2976	1.7658
.2664	1.8048
.2336	1.8458
.2000	1.8778
.1336	1.9271
.0664	1.9578
0	1.9764
-.0664	1.9930
-.1336	2.0032
-.2000	2.0090
-.6280	0
x = 7	
0.3896	0
-.3616	0
x = 8	
0.2752	0
-.1000	0

TABLE II.- PRESSURE-ORIFICE LOCATIONS

Gage number	x/c	s/D_n
Center line of lower surface		
1	0	0
2	.060	0
3	.123	0
4	.262	0
5	.373	0
6	.484	0
7	.625	0
8	.763	0
9	.886	0
Outboard ray on lower surface		
10	0.123	0.24
11	.262	.65
12	.373	1.01
13	.484	1.39
14	.625	1.78
15	.763	2.18
16	.886	2.55
Side of leading-edge surface		
17	0.123	1.08
18	.262	1.46
19	.373	1.91
20	.484	2.11
21	.625	2.44

Gage number	x/c	s/D_n
Ray on lower surface ahead of instrumented elevon		
22	0.623	1.22
23	.684	1.33
24	.736	1.44
25	.810	1.55
Without elevon deflection		
26	0.902	1.57
27	.925	1.57
28	.960	1.57
Elevon deflected, 15°		
26	0.902	1.57
27	.927	1.57
28	.964	1.57
Elevon deflected, 30°		
26	0.900	1.57
27	.930	1.57
28	.961	1.57
Leading edge of tip fin		
29	0.825	4.0
30	.907	4.34
31	.987	4.66

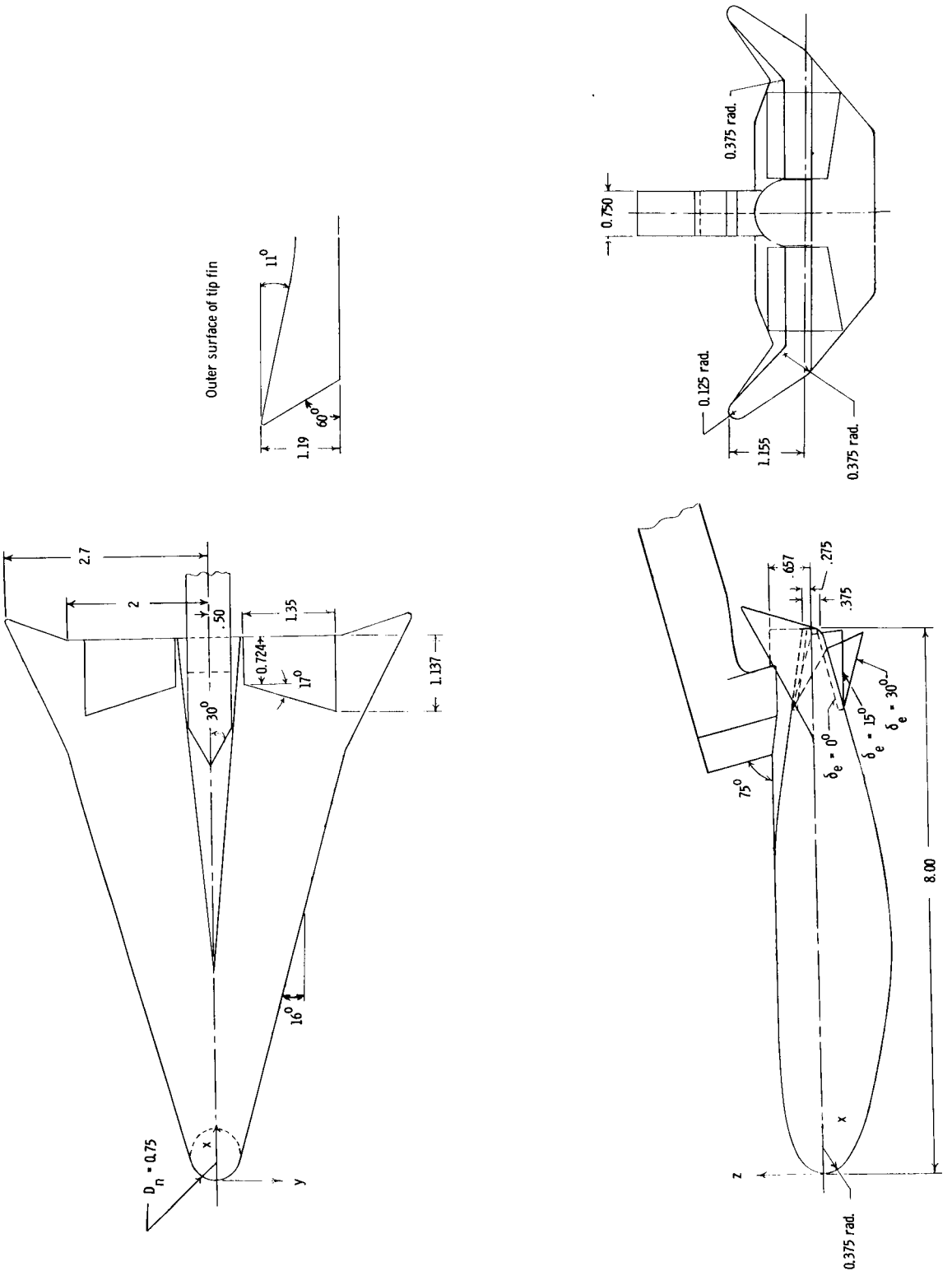

Figure 1.- Drawing of 8-inch HL-10 model. Dimensions are in inches unless otherwise noted.

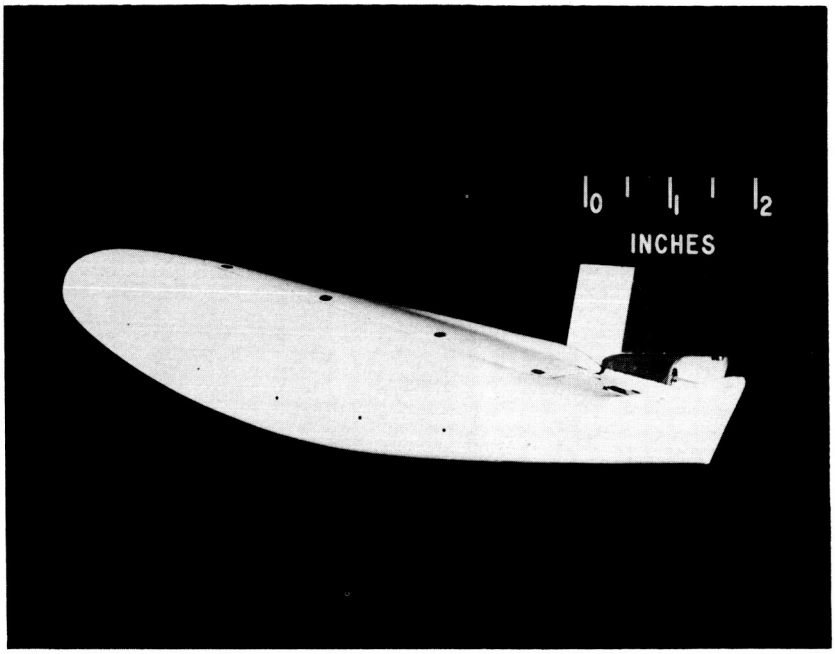

(a) Side view. L-64-11182

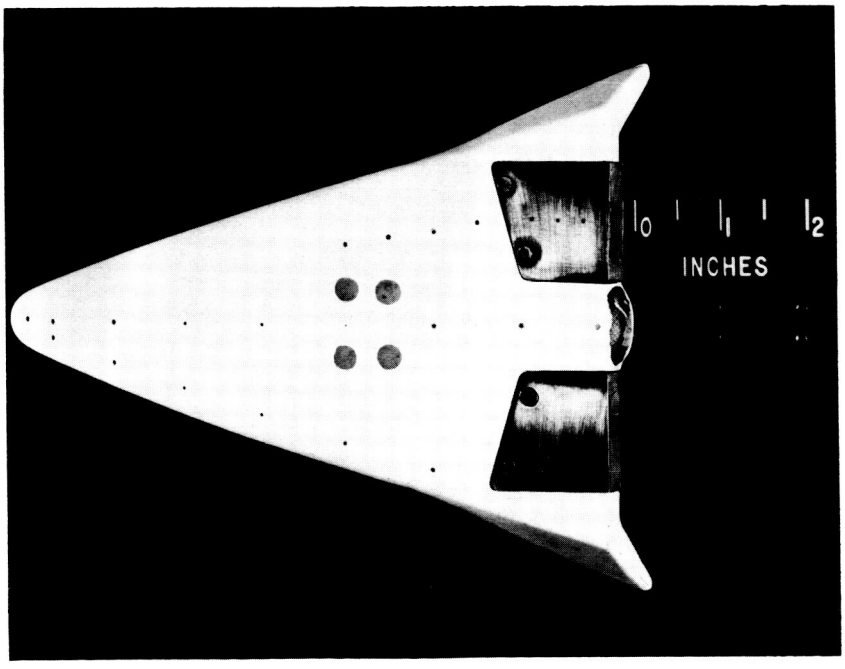

(b) Bottom view. L-64-11183

Figure 2.- Photographs of 8-inch HL-10 pressure model.

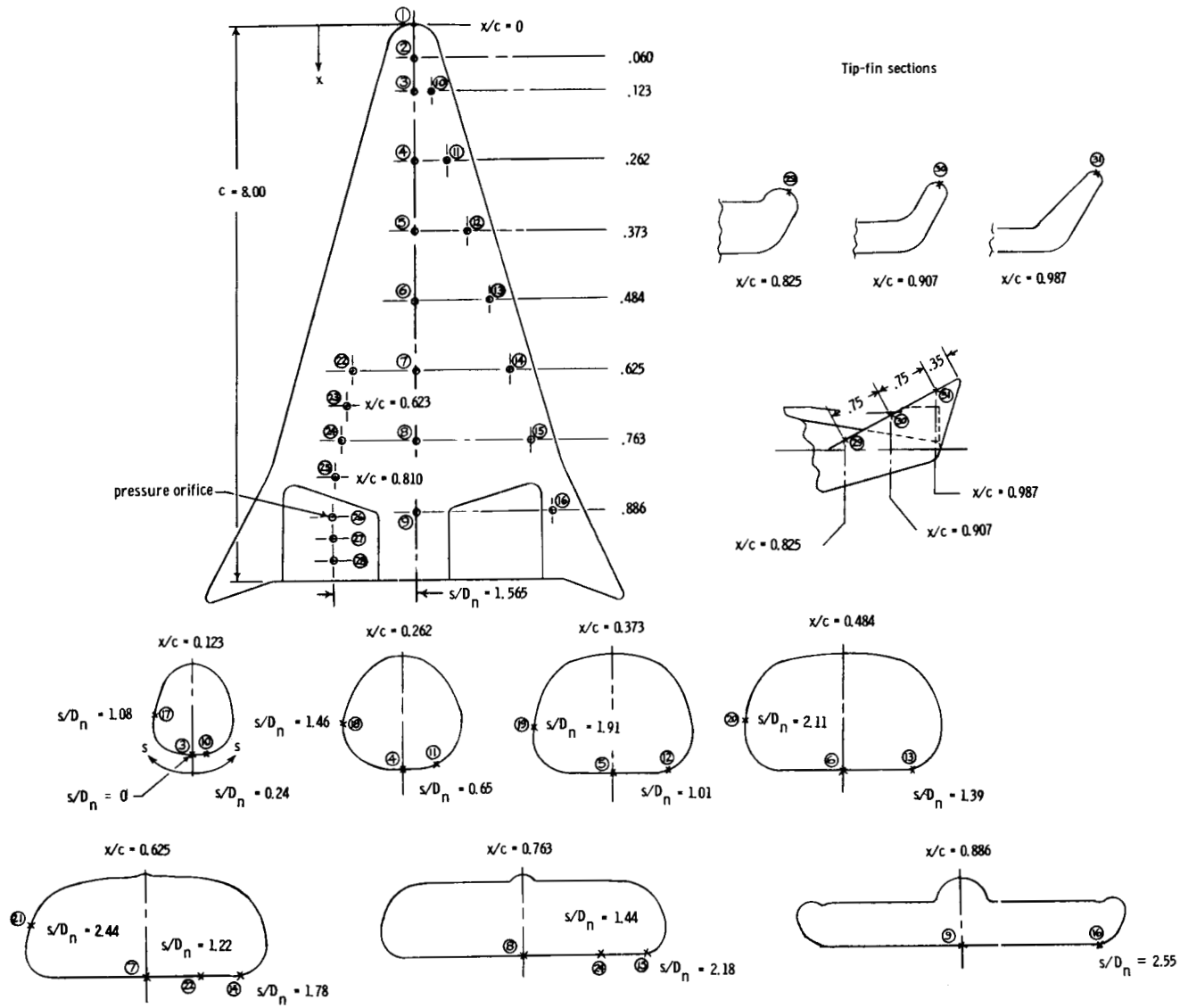

Figure 3.- Pressure-orifice locations for the HL-10 model. All dimensions are in inches. See table II for pressure-orifice coordinates for the elevon.

(a) $\delta_e = 15^o$; $\alpha = 50^o$.

(b) $\delta_e = 30^o$; $\alpha = 30^o$.

(c) $\delta_e = 30^o$; $\alpha = 40^o$.

(d) $\delta_e = 30^o$; $\alpha = 50^o$.

L-65-141

Figure 4.- Schlieren photographs.

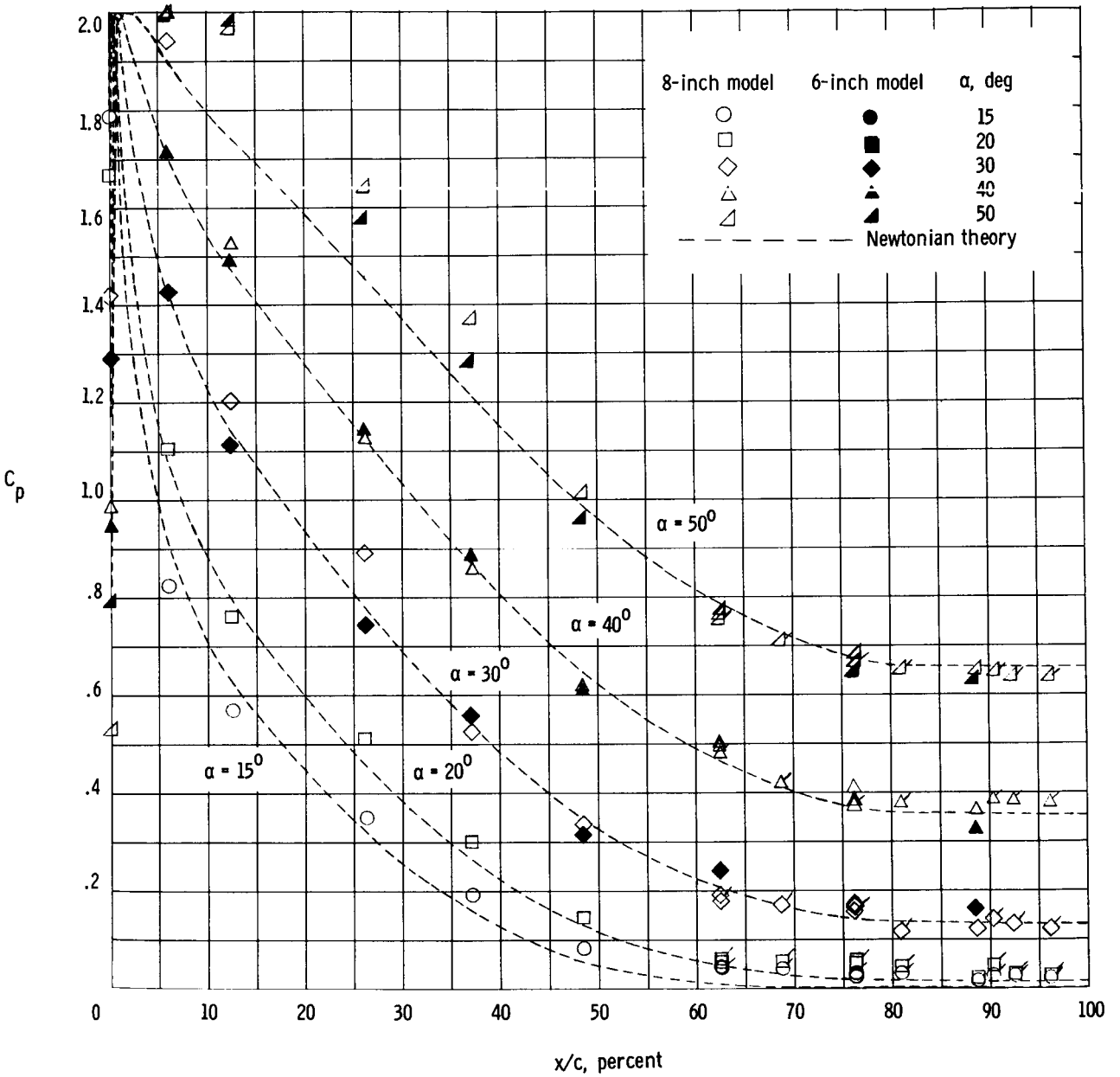

(a) Along center line, ray located ahead of elevon, and elevon.

Figure 5.- Chordwise pressure distribution on HL-10 model for an elevon deflection of 0°. Unflagged symbols are for gages 1 to 9; flagged symbols, for gages 22 to 28.

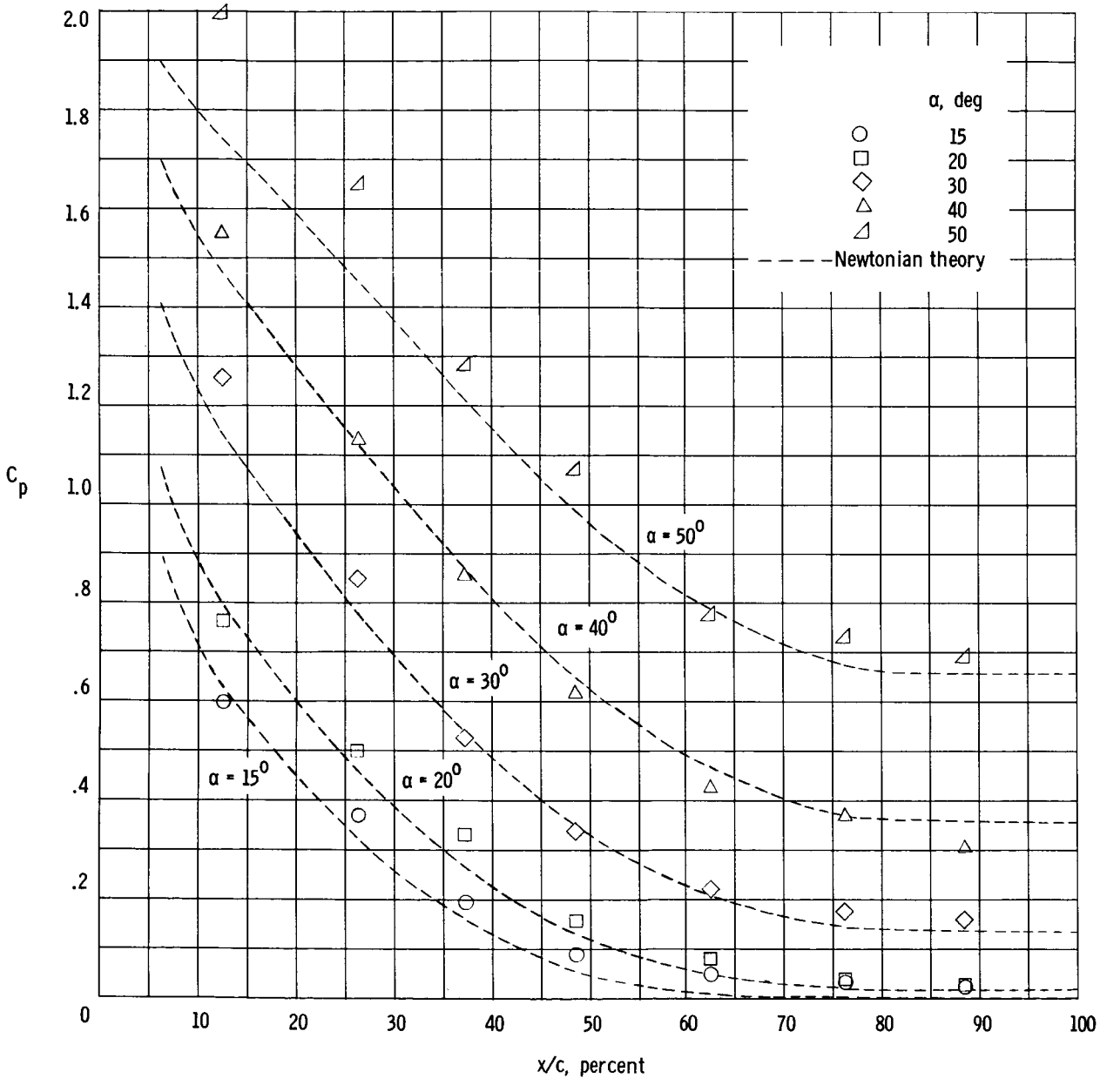

(b) Outboard ray; gages 10 to 16.

Figure 5.- Concluded.

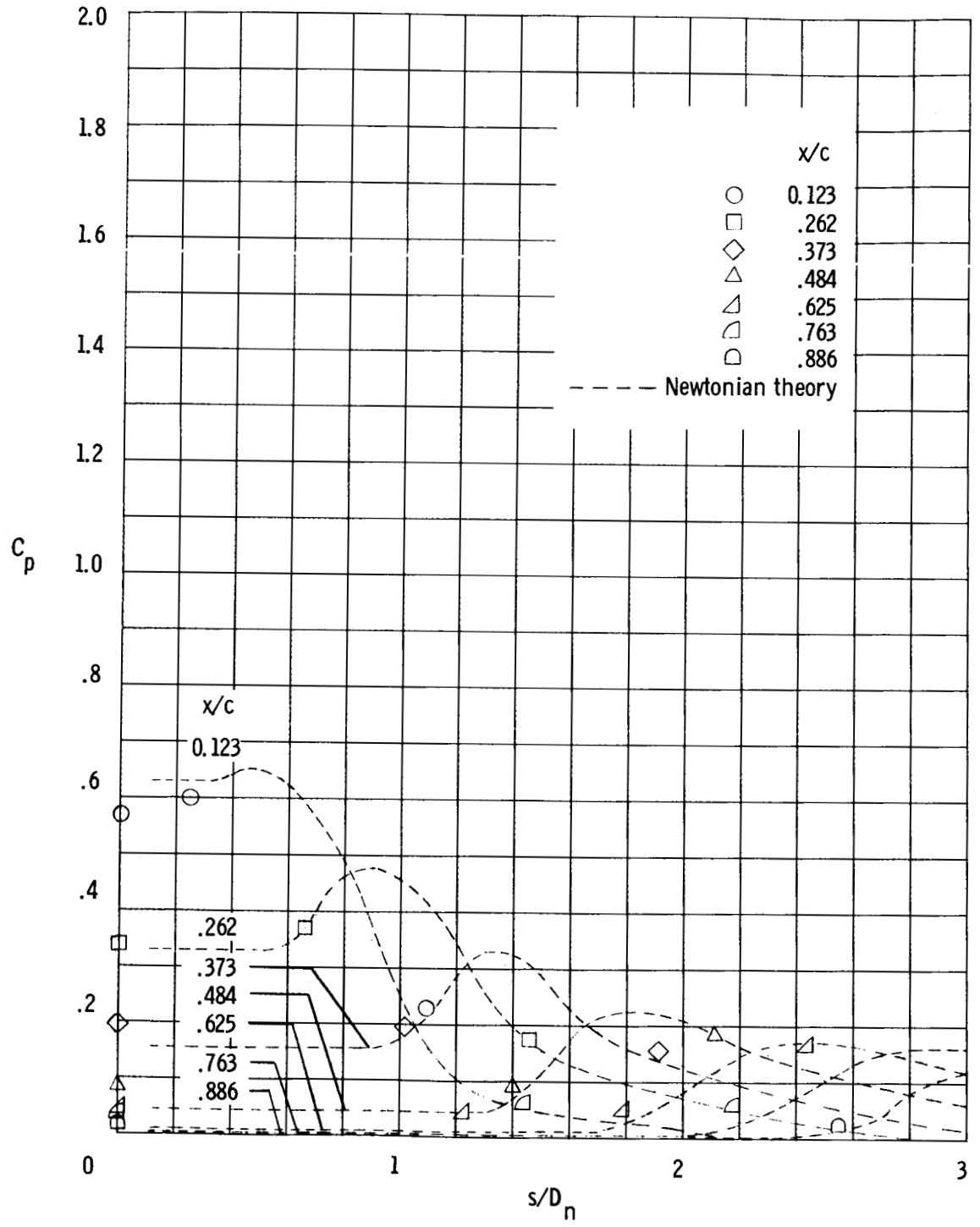

(a) $\alpha = 15^0$.

Figure 6.- Spanwise pressure distribution on HL-10 model for an elevon deflection of 0^0.

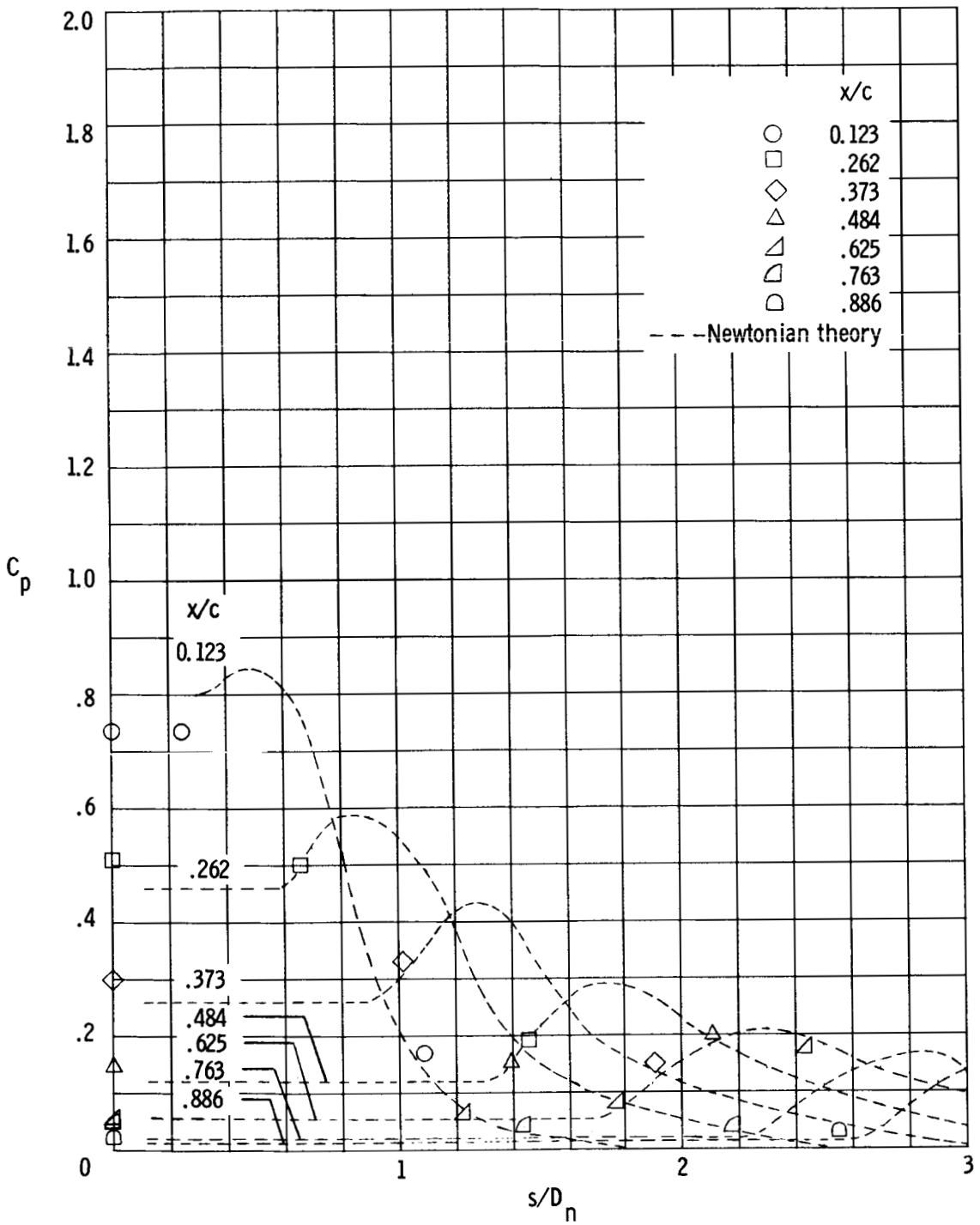

(b) $\alpha = 20^{\circ}$.

Figure 6.- Continued.

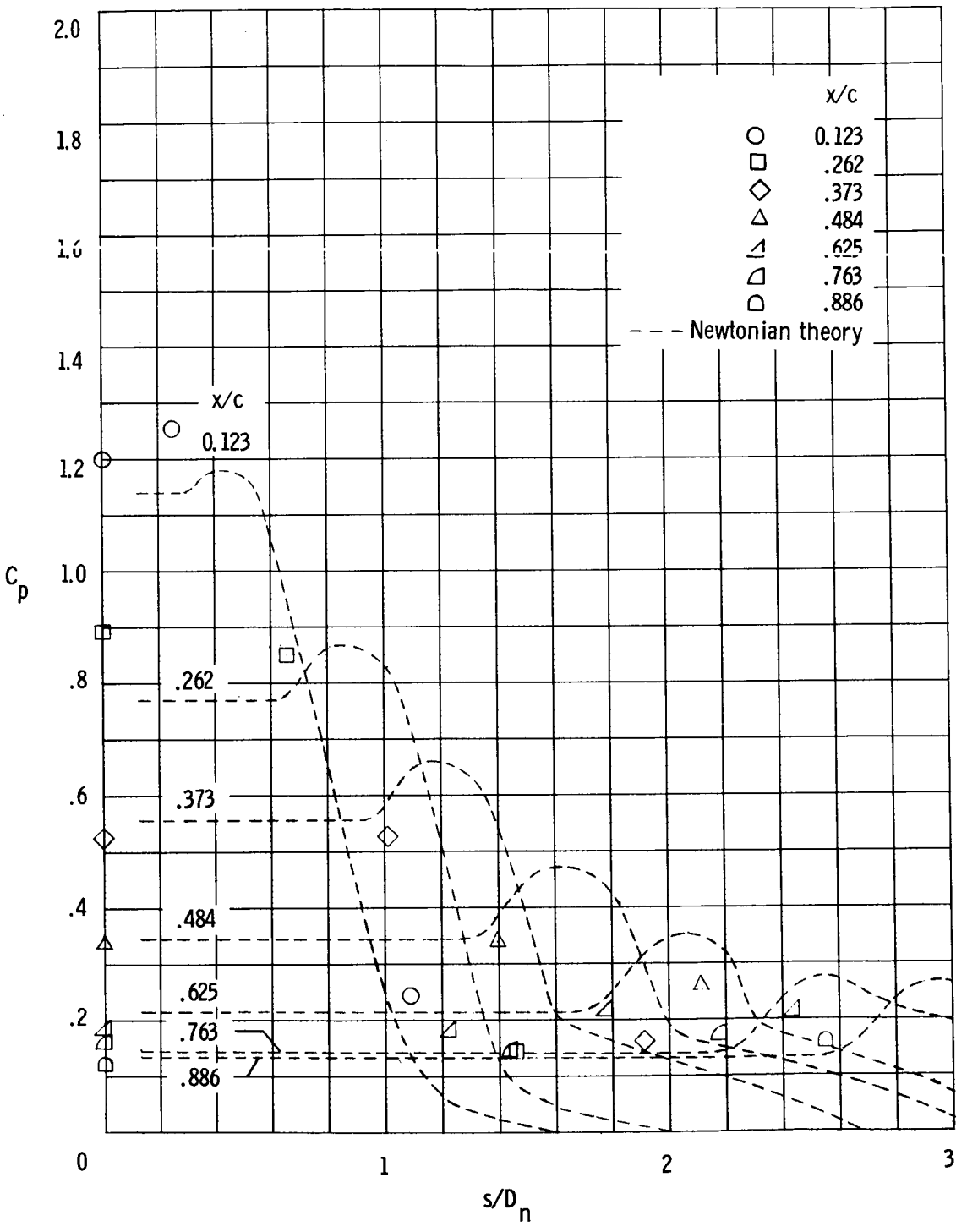

(c) $\alpha = 30^{\circ}$.

Figure 6.- Continued.

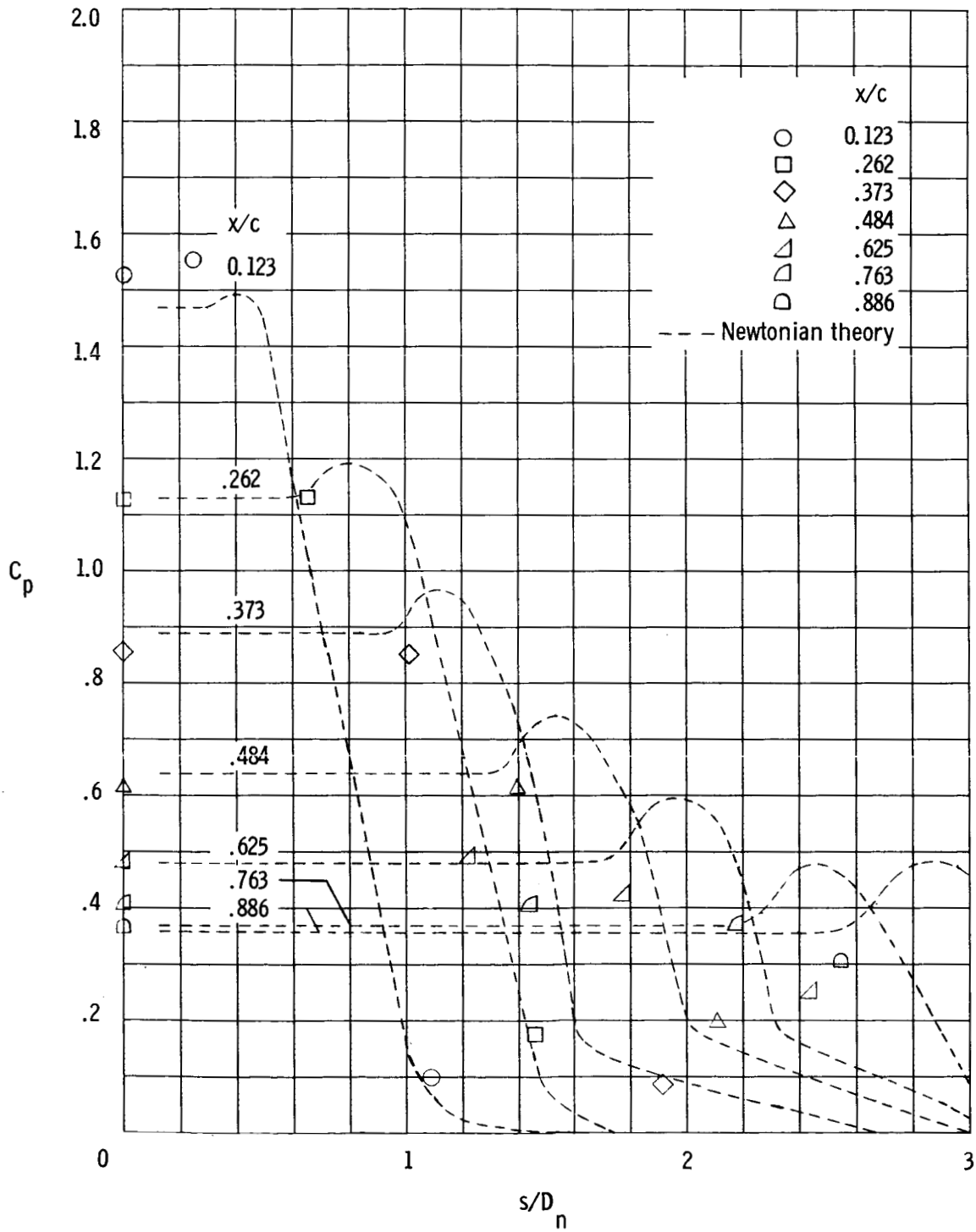

(d) $\alpha = 40^0$.

Figure 6.- Continued.

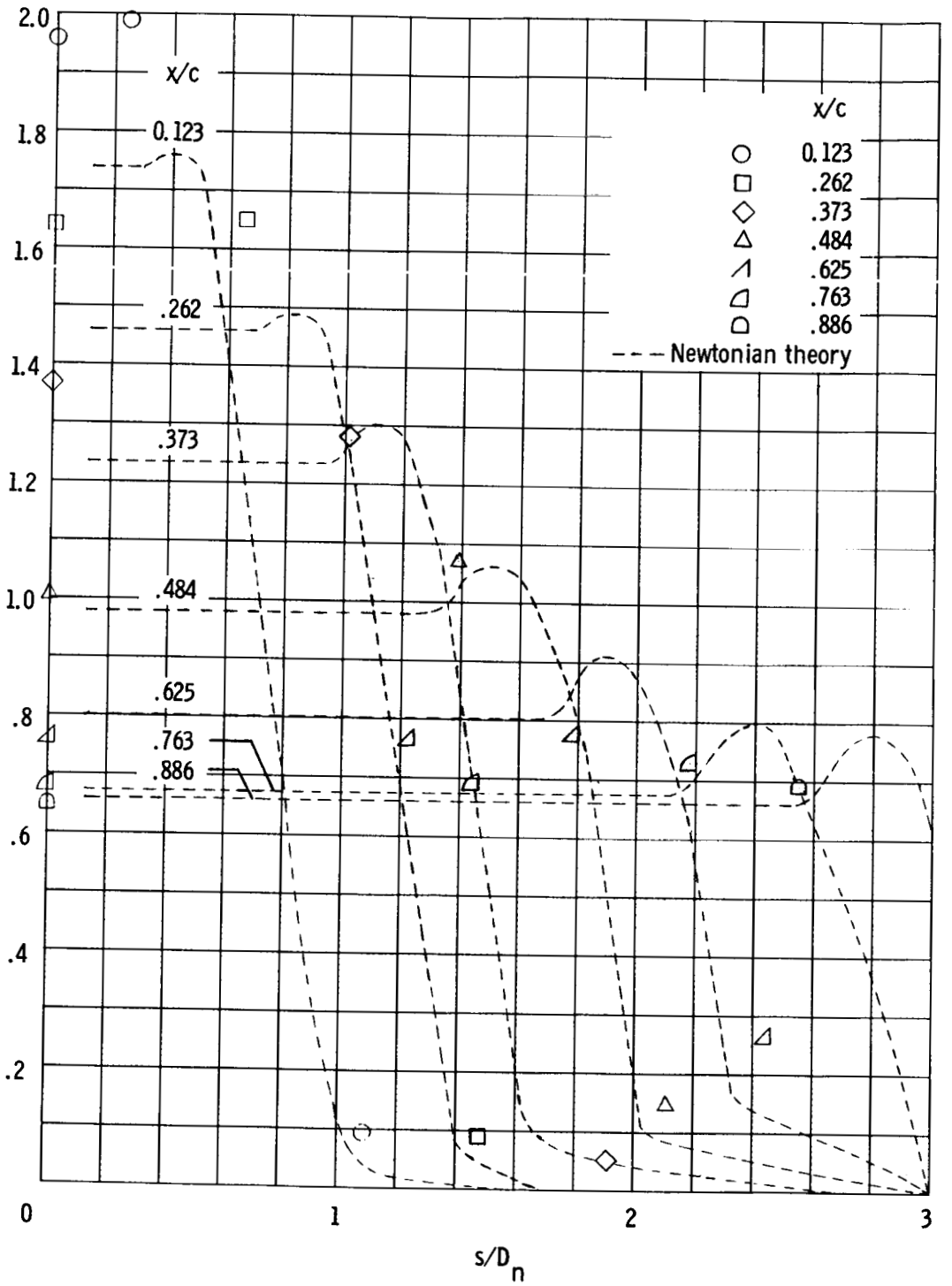

(e) $\alpha = 50^0$.

Figure 6.- Concluded.

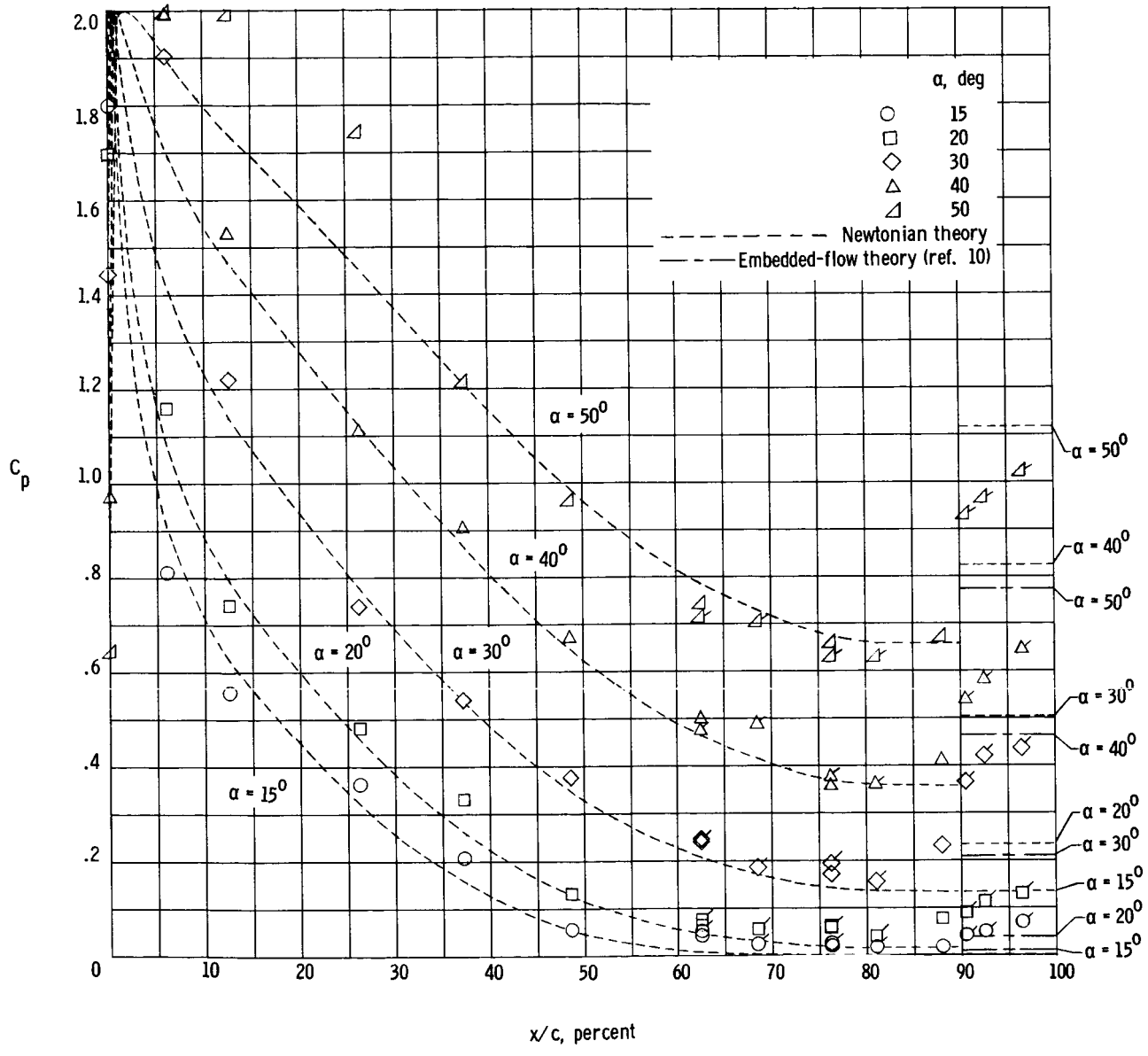

(a) Along center line, ray located ahead of elevon, and elevon.

Figure 7.- Chordwise pressure distribution on HL-10 model for an elevon deflection of 15°. Unflagged symbols are for gages 1 to 9; flagged symbols, for gages 22 to 28.

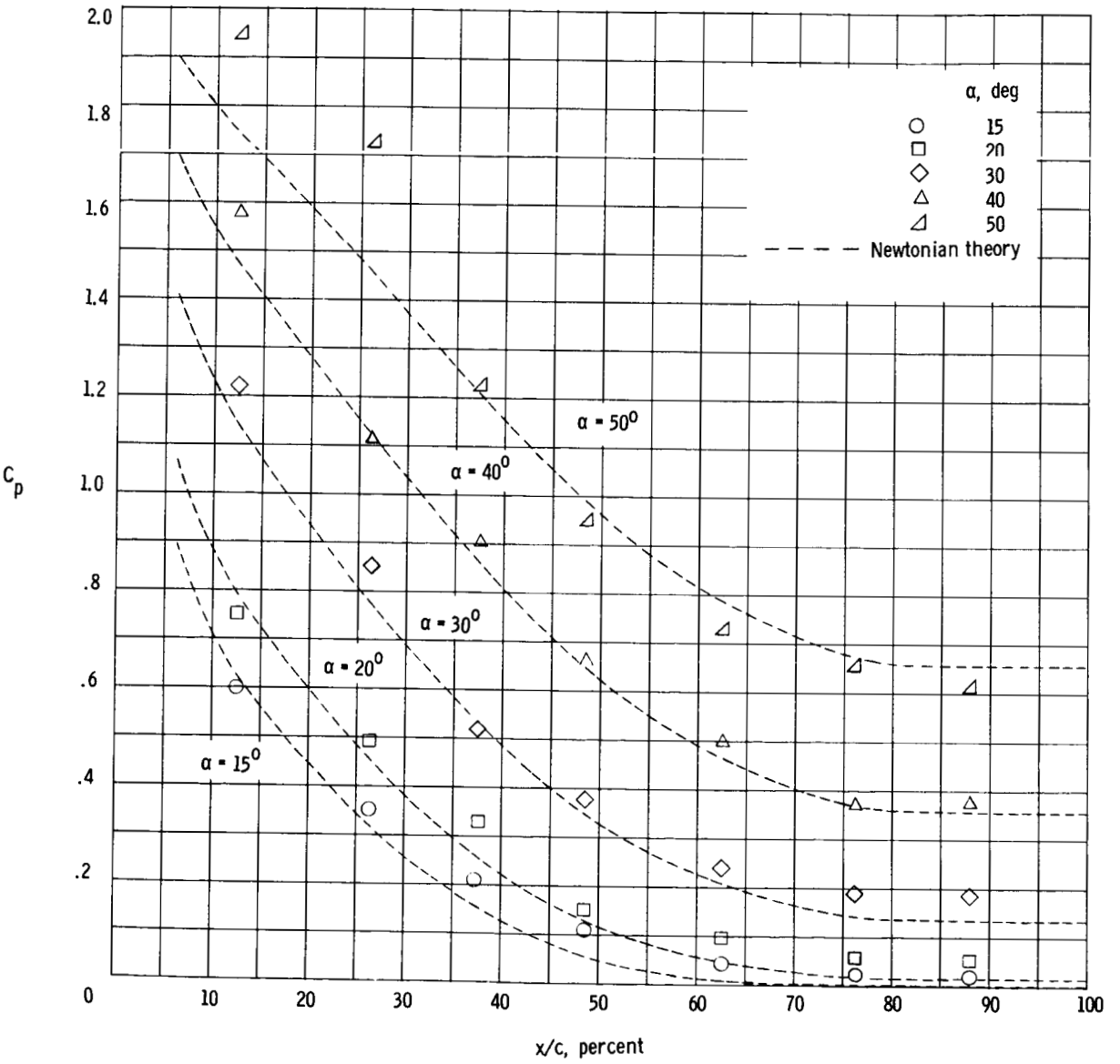

(b) Outboard ray; gages 10 to 16.

Figure 7.- Concluded.

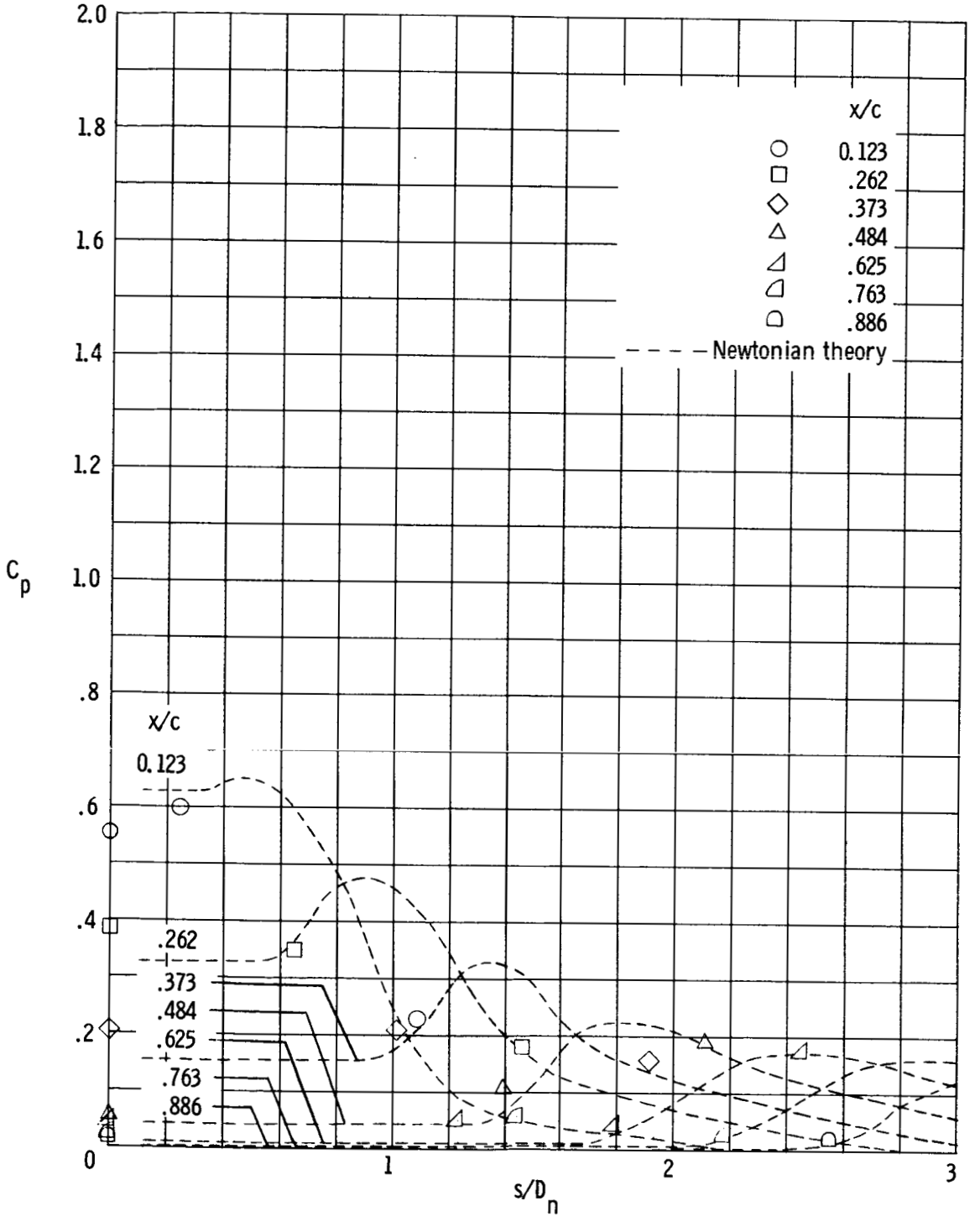

(a) $\alpha = 15^0$.

Figure 8.- Spanwise pressure distribution on HL-10 model for an elevon deflection of 15^0.

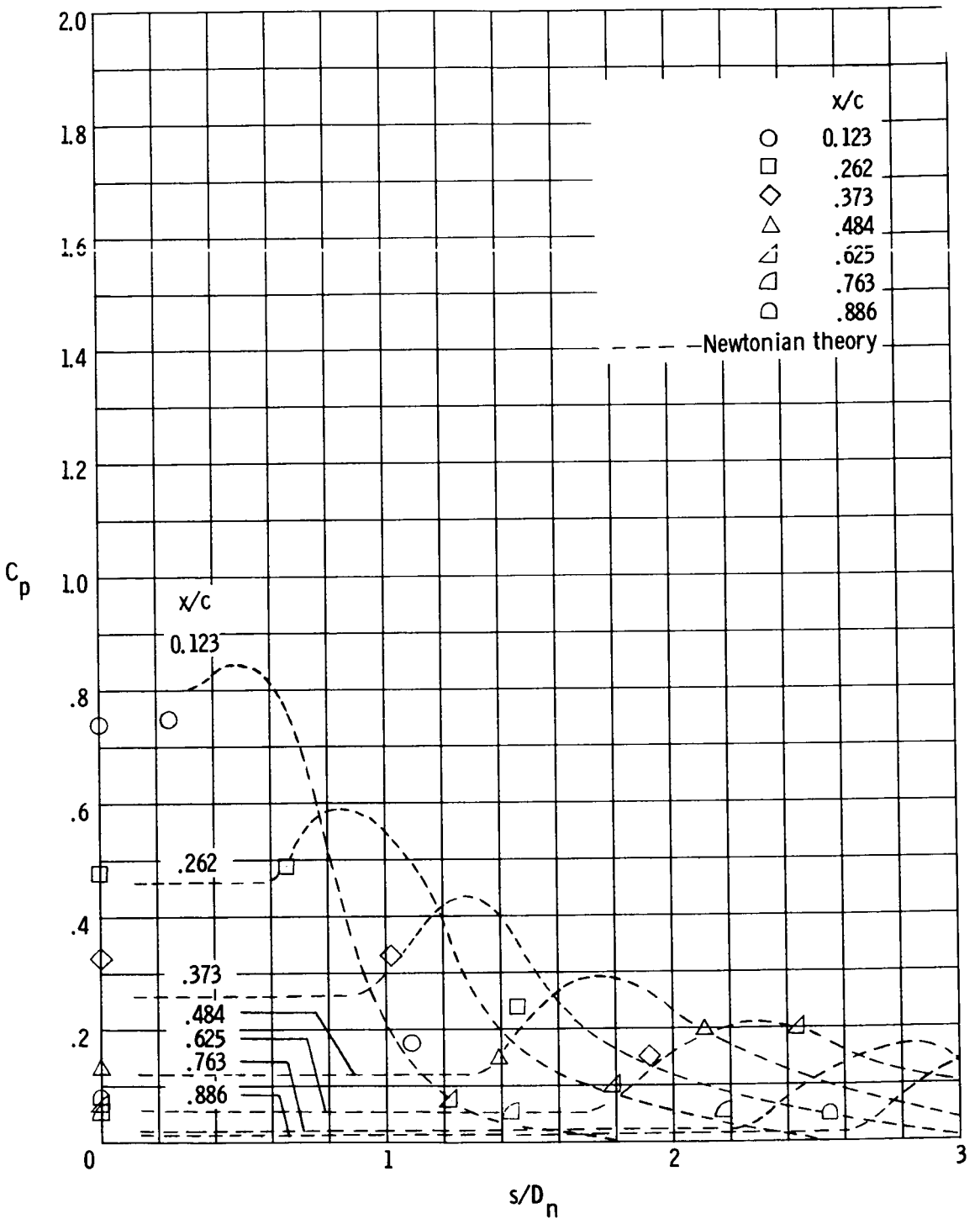

(b) $\alpha = 20^{\circ}$.

Figure 8.- Continued.

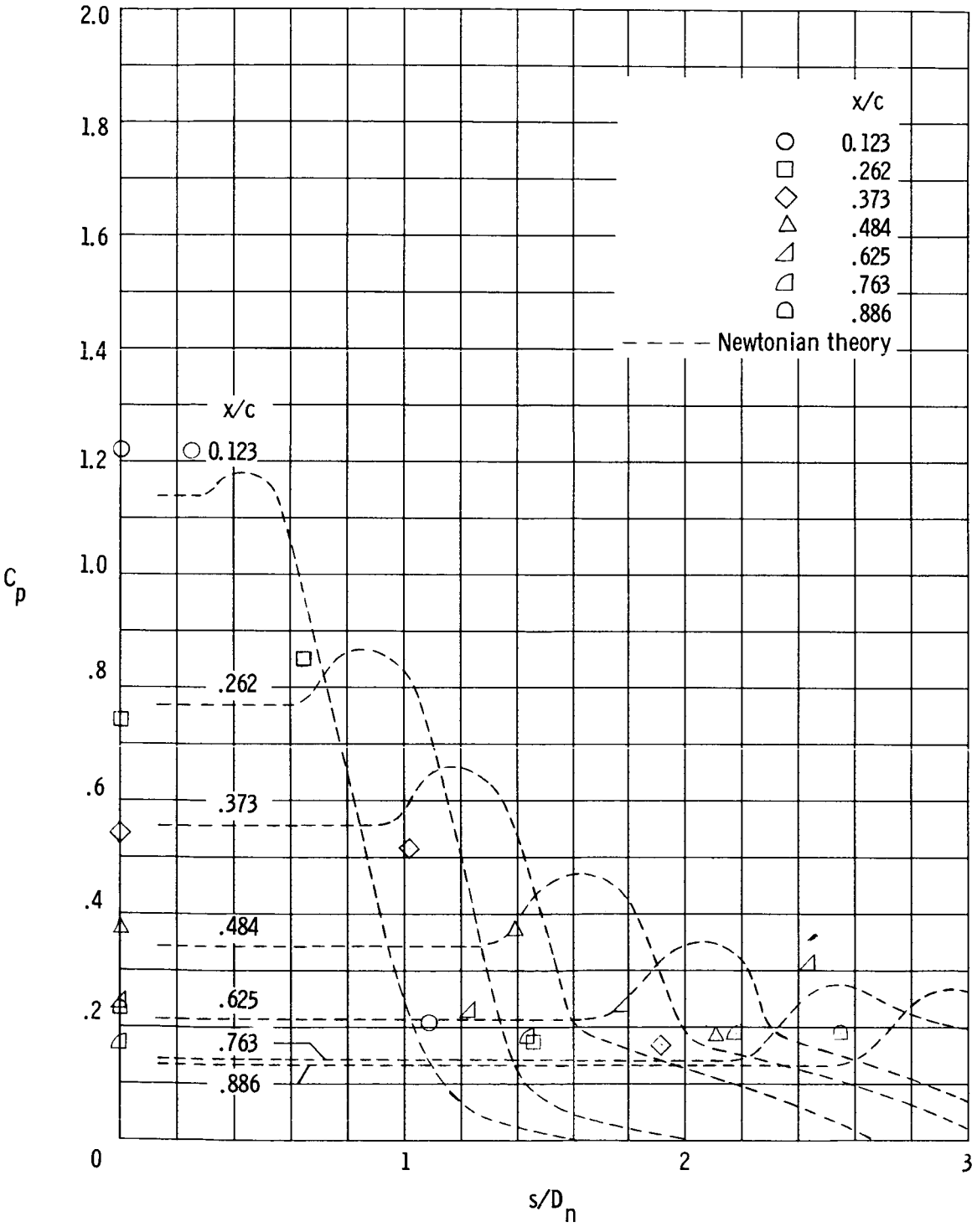

(c) $\alpha = 30^0$.

Figure 8.- Continued.

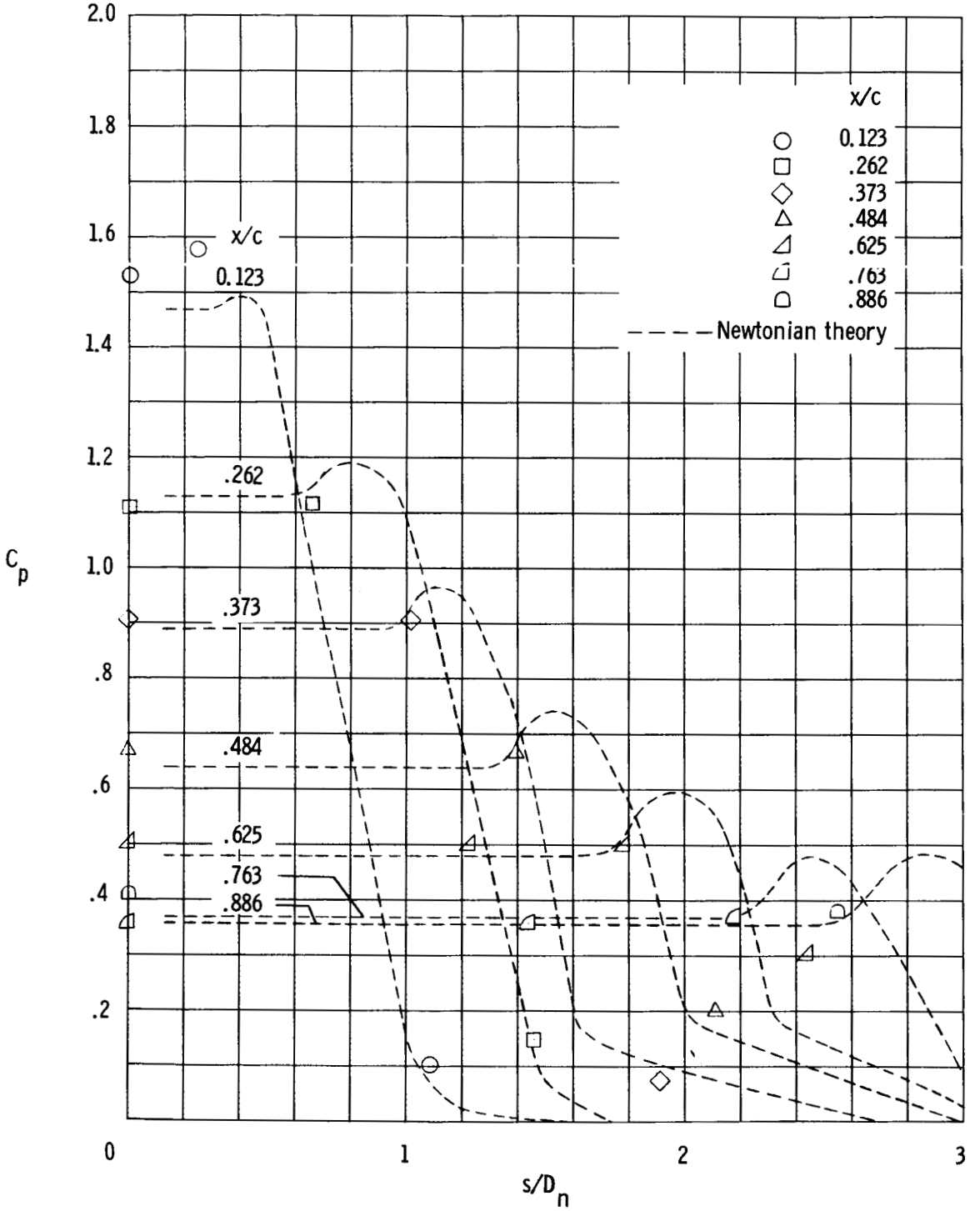

(d) $\alpha = 40^{\circ}$.

Figure 8.- Continued.

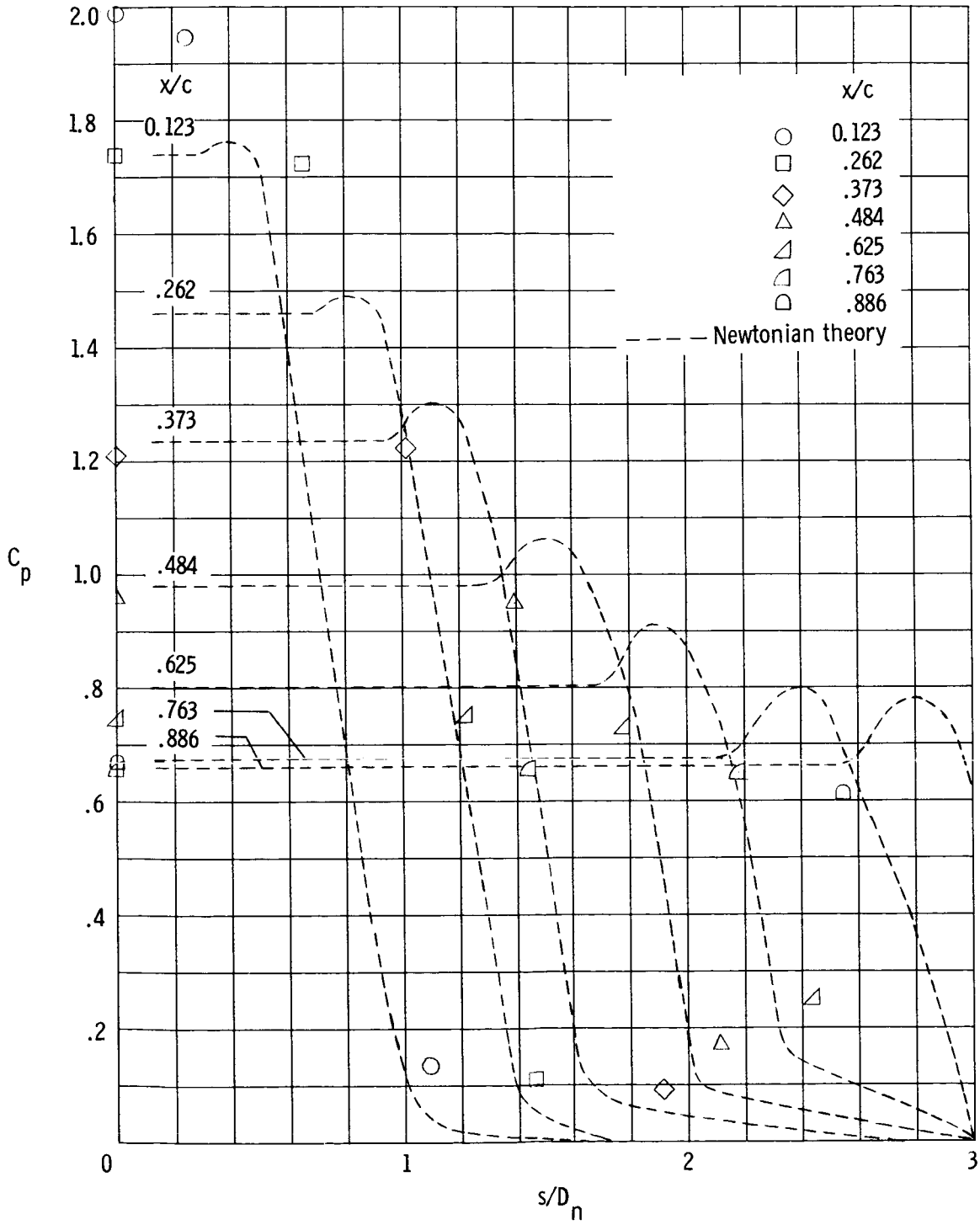

(e) $\alpha = 50^0$.

Figure 8.- Concluded.

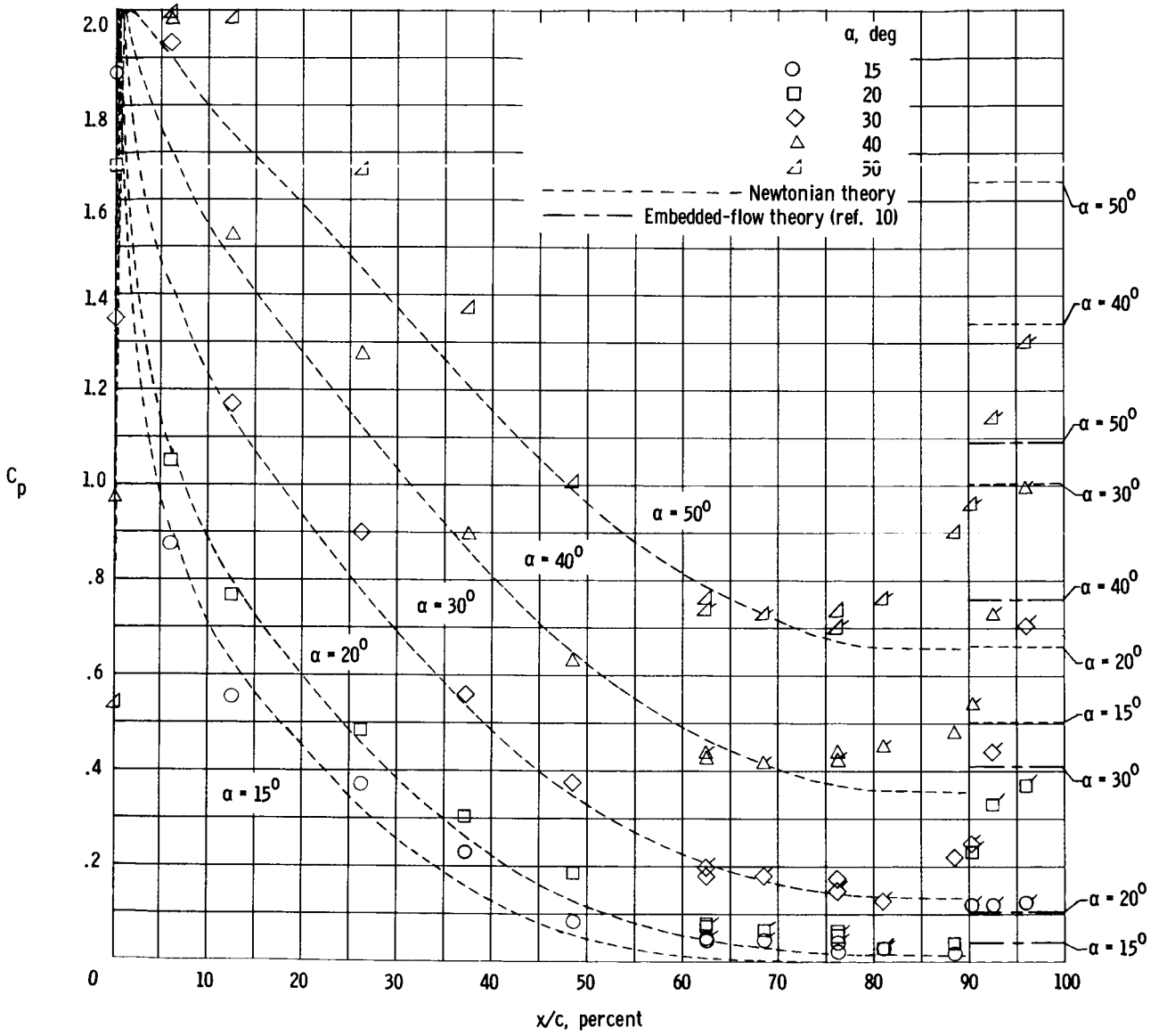

(a) Along center line, ray located ahead of elevon, and elevon.

Figure 9.- Chordwise pressure distribution on HL-10 model for an elevon deflection of 30°. Unflagged symbols are for gages 1 to 9; flagged symbols, for gages 22 to 28.

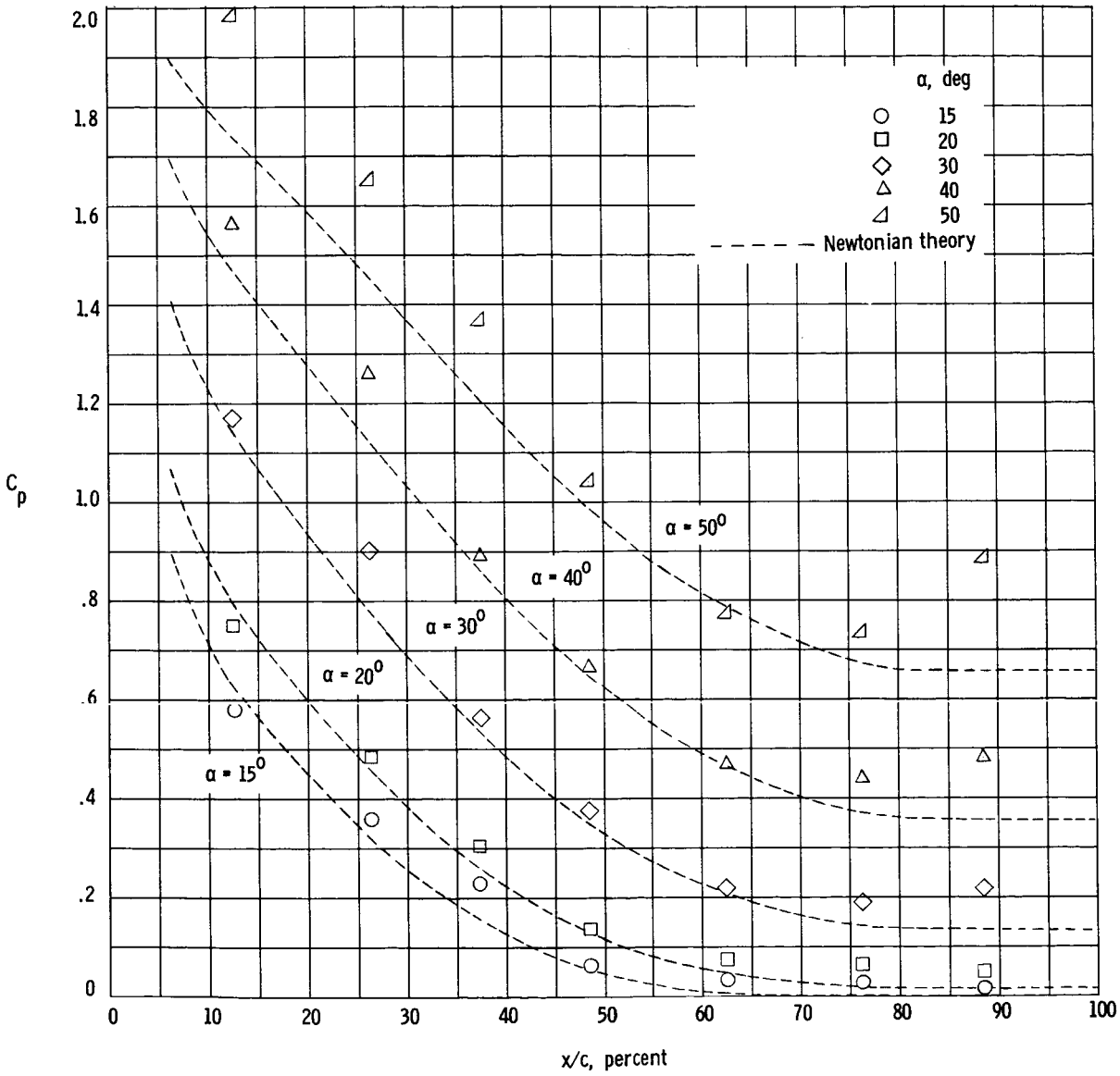

(b) Outboard ray; gages 10 to 16.

Figure 9.- Concluded.

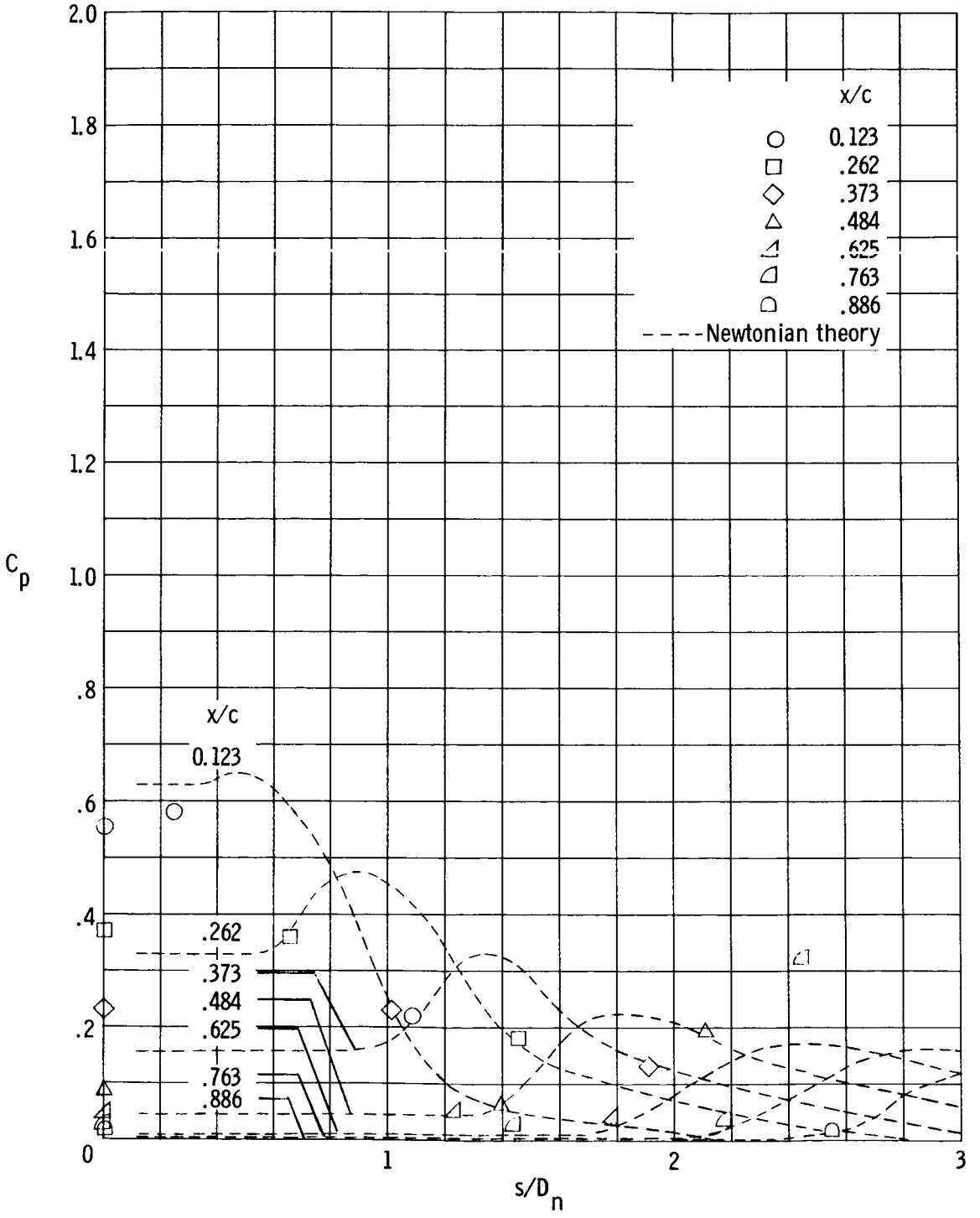

(a) $\alpha = 15^0$.

Figure 10.- Spanwise pressure distribution on HL-10 model for an elevon deflection of 30^0.

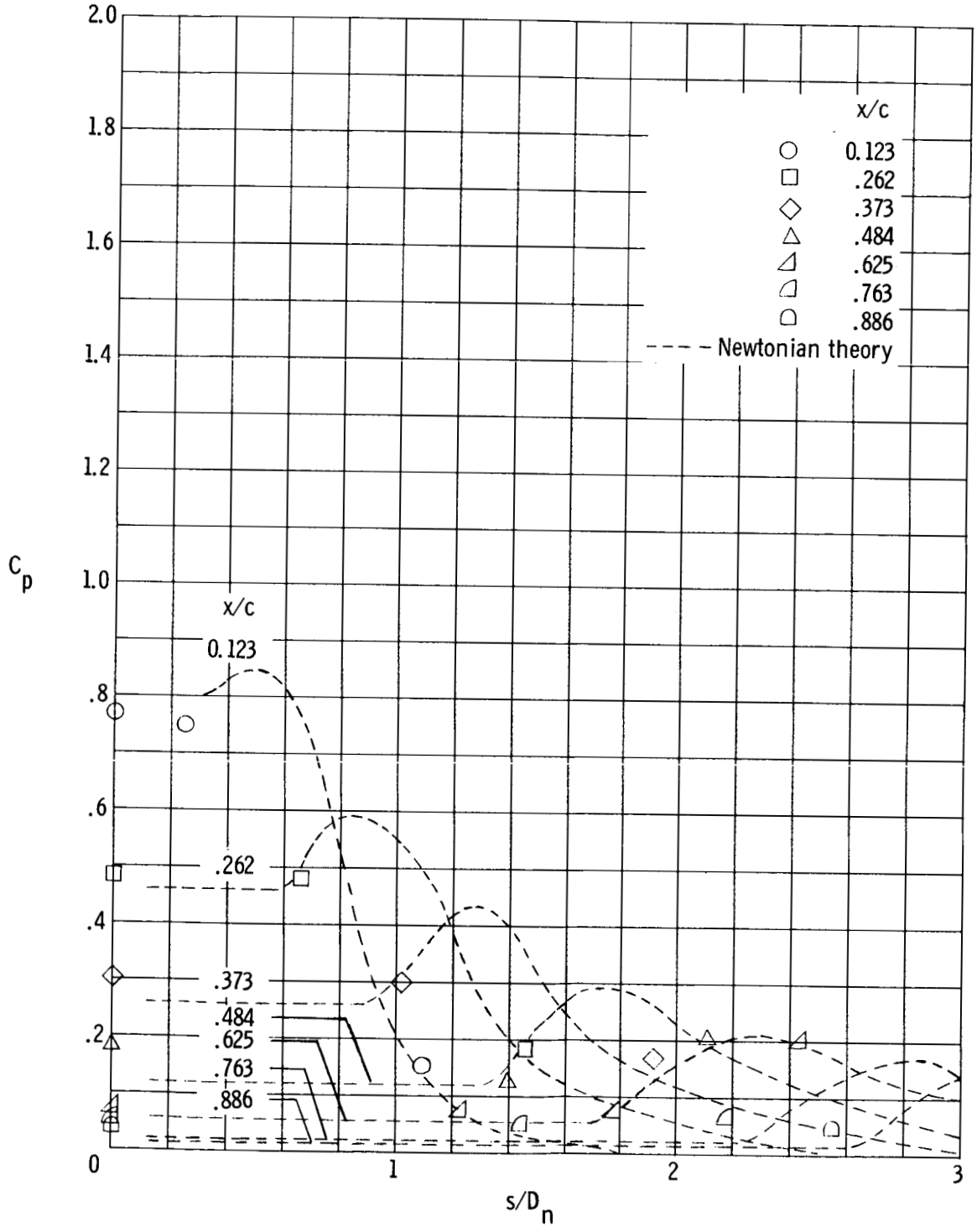

(b) $\alpha = 20^{\circ}$.

Figure 10.- Continued.

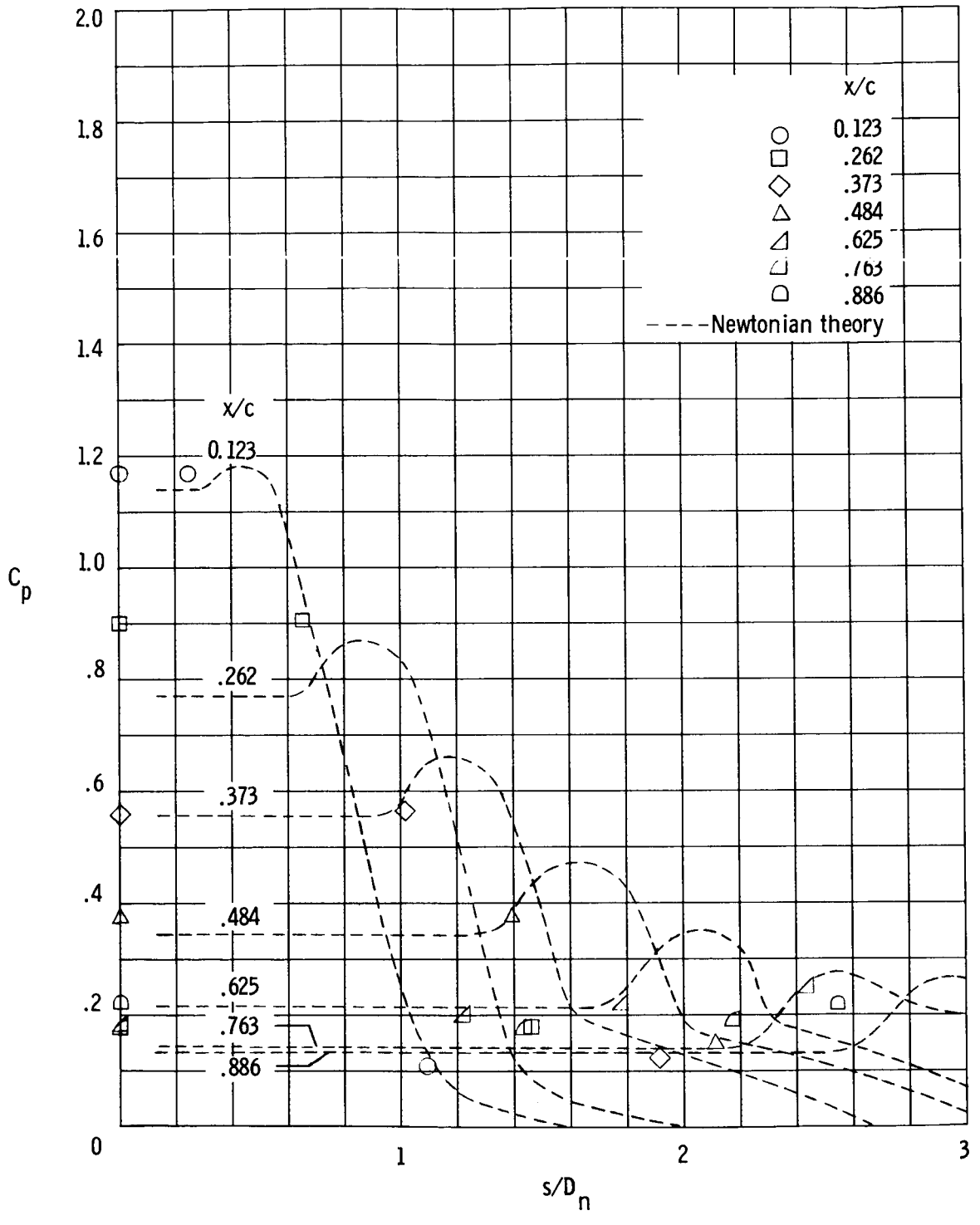

(c) $\alpha = 30^{0}$.

Figure 10.- Continued.

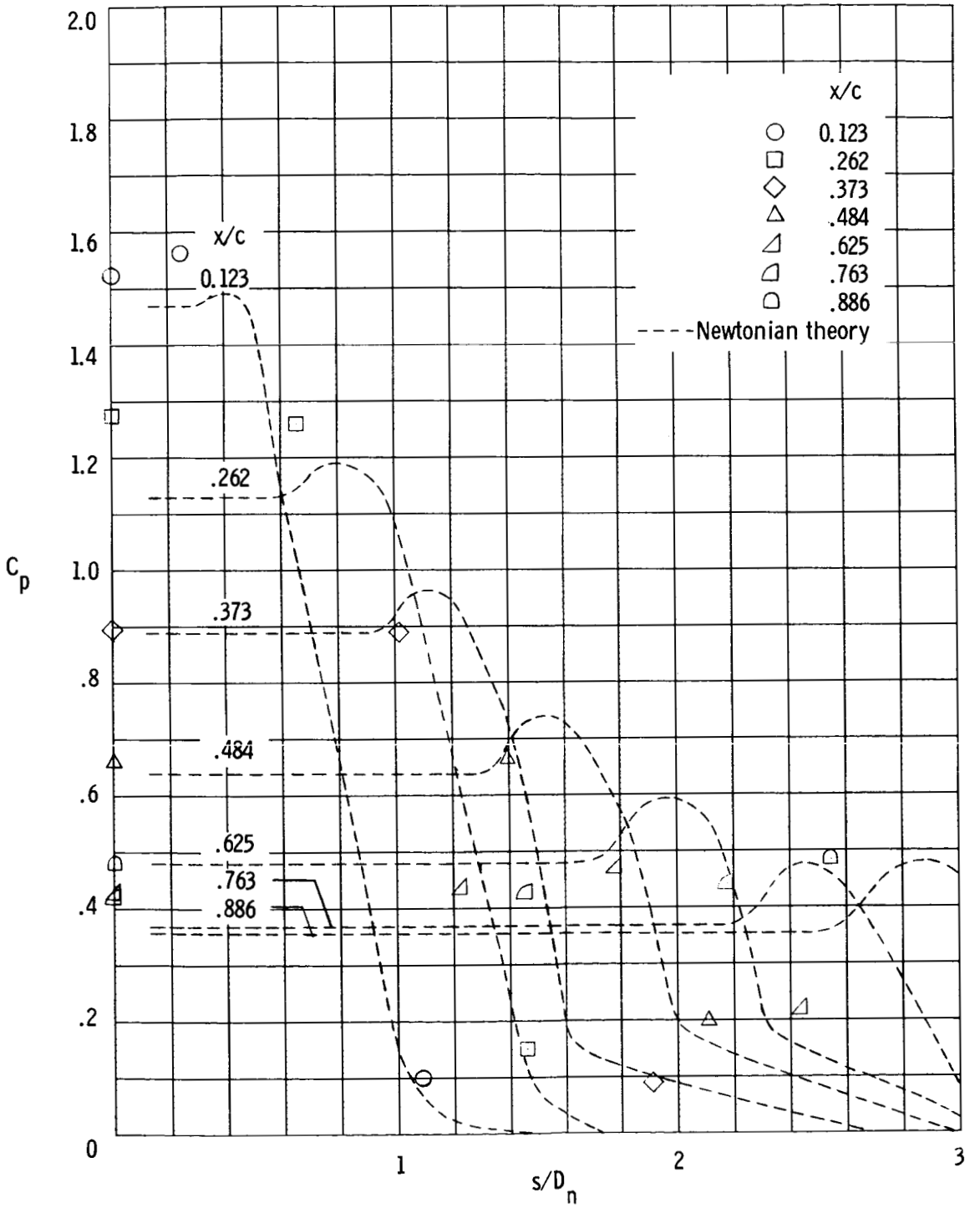

(d) $\alpha = 40^{\circ}$.

Figure 10.- Continued.

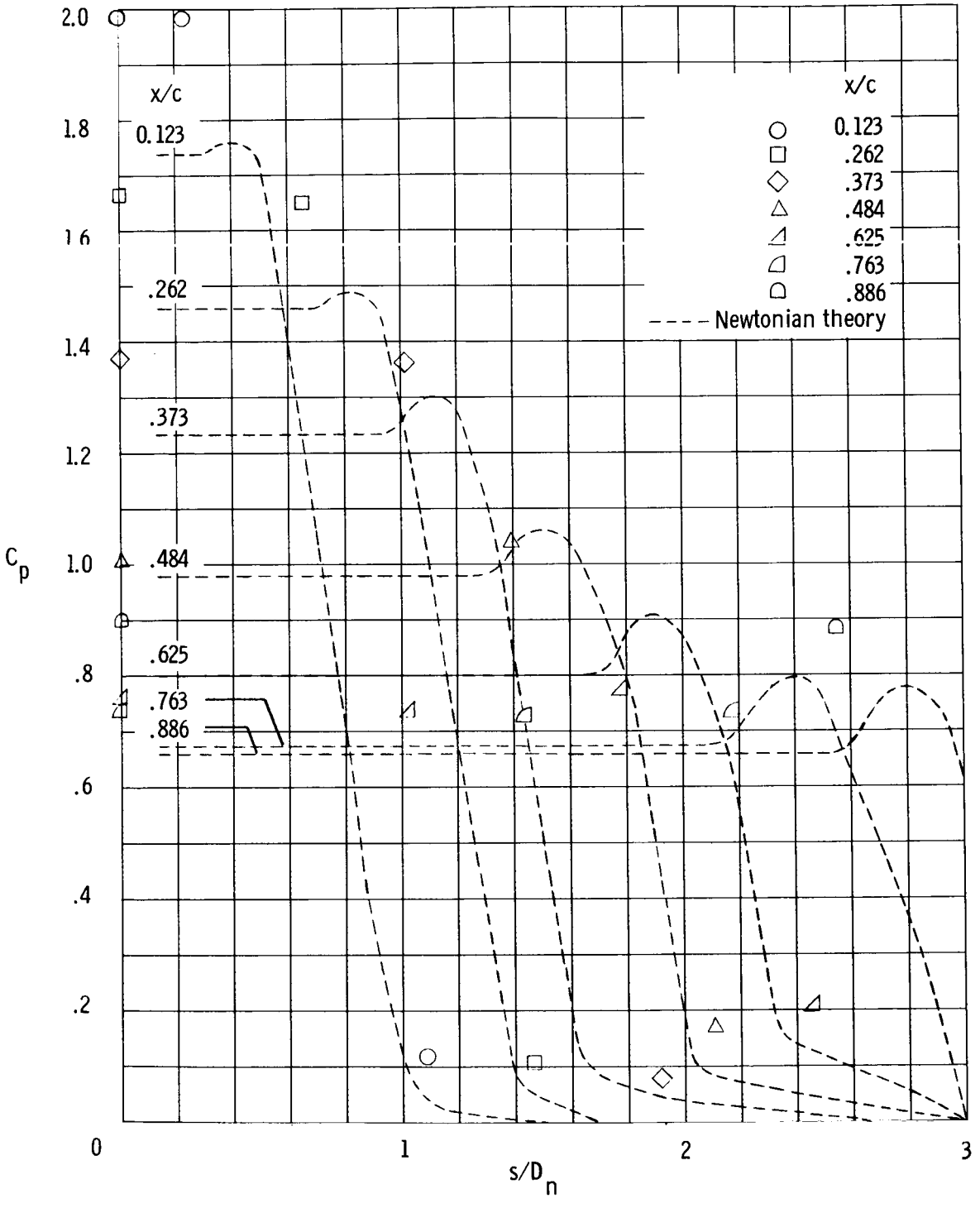

(e) $\alpha = 50^{\circ}$.

Figure 10.- Concluded.

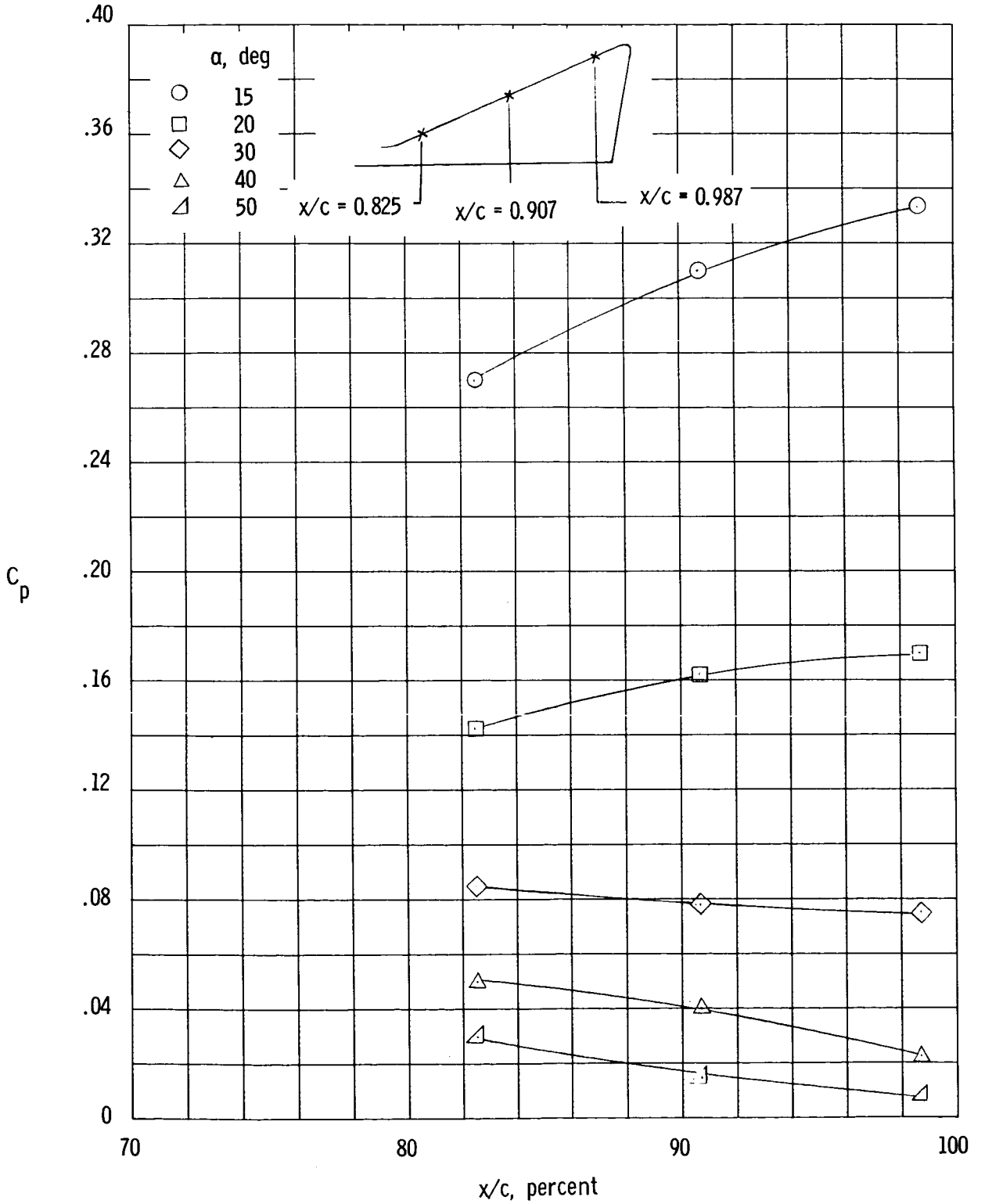

Figure 11.- Tip-fin leading-edge pressure distribution.

"The aeronautical and space activities of the United States shall be conducted so as to contribute . . . to the expansion of human knowledge of phenomena in the atmosphere and space. The Administration shall provide for the widest practicable and appropriate dissemination of information concerning its activities and the results thereof."

—NATIONAL AERONAUTICS AND SPACE ACT OF 1958

NASA SCIENTIFIC AND TECHNICAL PUBLICATIONS

TECHNICAL REPORTS: Scientific and technical information considered important, complete, and a lasting contribution to existing knowledge.

TECHNICAL NOTES: Information less broad in scope but nevertheless of importance as a contribution to existing knowledge.

TECHNICAL MEMORANDUMS: Information receiving limited distribution because of preliminary data, security classification, or other reasons.

CONTRACTOR REPORTS: Technical information generated in connection with a NASA contract or grant and released under NASA auspices.

TECHNICAL TRANSLATIONS: Information published in a foreign language considered to merit NASA distribution in English.

TECHNICAL REPRINTS: Information derived from NASA activities and initially published in the form of journal articles.

SPECIAL PUBLICATIONS: Information derived from or of value to NASA activities but not necessarily reporting the results of individual NASA-programmed scientific efforts. Publications include conference proceedings, monographs, data compilations, handbooks, sourcebooks, and special bibliographies.

Details on the availability of these publications may be obtained from:

SCIENTIFIC AND TECHNICAL INFORMATION DIVISION

NATIONAL AERONAUTICS AND SPACE ADMINISTRATION

Washington, D.C. 20546